Design, modeling and implementation of a biphasic media variable stiffness actuator

UNIVERSITÀ DEGLI STUDI DI GENOVA

Jesus Hiram LUGO CALLES

Department of Mechanical Engineering

University of Genoa, Italy

This dissertation is submitted for the degree of

Doctor of Philosophy

February 5, 2019

Acknowledgements

Firstly, I would like to thank Prof. Matteo Zoppi for being my thesis supervisor, always providing continuous support and ideas for the project.

I would like to acknowledge Prof. Giorgio Cannata for helping me during the control design of this project, making himself available for meetings and experiments as much as needed.

I would like to credit Prof. Rezia Molfino for giving me the opportunity to participate in different activities related to my research.

I would like to express my gratitude to my fellow laboratory mates Keerthi, Cuong, Vishal, Ahmad, Sadiq, Mikka and Giorgio for their friendship and support during my stay. I am thankful to Alessio Caligiuri for helping me to develop the most important part of the project. I would like to thank my family and my Cristina for being supportive all these years.

I appreciate the support, the space and funding of the Department of Mechanical Engineering from the University of Genoa. Finally, I would like to thank the National Council of Science and Technology (CONACYT) for their support and sponsorship for the realization of this thesis.

Abstract

Nowadays, an increasing number of industrial processes are expected to have robots interacting safely with humans and the environment. Compliance control of robotic systems strongly addresses these scenarios. This thesis develops a variable stiffness actuator (VSA) whose position and stiffness can be controlled independently. Actuator's stiffness is controlled by changing pressure of control fluid into distribution lines. The used control fluid is biphasic, composed of separated gas and liquid fractions with predefined ratio. Firstly, an approach for the mathematical model is introduced and a model-based control method is implemented to track the desired position and stiffness. Results from force loaded and unloaded simulations proved the feasibility of these methods. Based on the previous outcome, a compliant revolute joint mechanism was modeled and implemented in order to use it as a test bench for the VSA. The mechanism is able to track position and stiffness accurately; however, better mechanical design and manufacturing methods are suggested in order to avoid excessive friction. Later on, a momentum-based collision detection and reaction algorithm is proposed, simulated and tested on the mechanism. Experimental results confirm that this method can be used to attain a higher level of safety in the system. Finally, a compliant cable-driven revolute joint using biphasic media variable stiffness actuators is modeled and simulated. This cable-driven mechanism is characterized by a wide range of stiffness and high-power output.

Contents

List of Figures

List of Tables

List of Abbreviations

ANSI American National Standards Institute. 2

BMVSA Biphasic media variable stiffness actuator. 1, 7, 10, 11, 20, 28, 50, 56, 68

cobot Cooperative robot. 3, 4, 32, 68

DOF degree of freedom. 10

HPA hydropneumatic accumulator. 14–16, 18, 21, 29, 44, 68

HPS hydropneumatic suspension. 14–16

HRI Human-robot interaction. iii, 3

ISO International Organization for Standardization. 2–4

MBCDA momentum-based collision detection algorithm. 52, 53, 56

N Nitrogen. 13, 14

PAM Pneumatic artificial muscles. 8

pHRI physical human-robot interaction. 3, 49, 68

PID Proportional Integral Derivative. 23, 24

SEA Series elastic actuator. 7, 8

VIA Variable impedance actuator. 5

VSA Variable stiffness actuator. iii, vi, 1, 5–7, 9, 10, 32, 33, 49, 68, 69, 75

VSD Variable stiffness device. 6

Chapter 1

Introduction

The problem of controlling stiffness in actuators appears when a robot is needed to perform motion tasks in the presence of humans, or when collisions with the environment are possible. For these scenarios, velocity and position should be sufficiently accurate while minimizing the risk of damaging humans, environment and itself [1, 2]. This need for safety is extended to unintended interactions due to hardware failure, limitations on perception and cognition.

A compliant system holds improved open loop characteristics by reducing the reflected inertia on the contact side of the impact [3]. A VSA is a device that allows deviations from its own equilibrium position, depending on the applied external force. The equilibrium position is defined as the position where the VSA generates zero net force or net torque [1, 4].

Mechanical impedance is defined as a dynamic relationship that generates a force as a function of displacement (in time), while admittance is its complement. Stiffness is the differential relation between infinitesimal differences in force and position, having compliance complementing it [1]. It is worthy of note that adjustable compliance, variable compliance and adjustable stiffness are used to describe an actuator with variable stiffness [4].

This thesis is based on Biphasic media variable stiffness actuator (BMVSA) technology, a VSA approach proposed and patented by PMAR Robotics Laboratory in 2012.

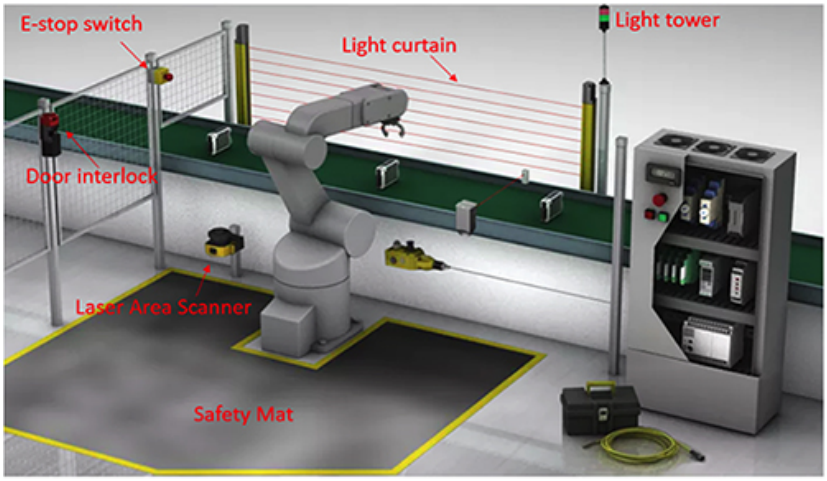

Figure 1.1: Typical industrial robotic cell setup. A variety of sensors is used to detect the presence of humans and shut down the system independently [6]

1.1 Safety in robotics

Nowadays, there is an increasing need for autonomous flexible machines that are able to efficiently adapt to a new process. The inclusion of robots to industrial environments has created production solutions characterized by high quality, low cost, improved ergonomics, and faster working cycles [5]. A robot can pose danger due to its speed, type of movement, force, and power supply. In order to protect workers from these threats, it is common to use barrier guards around the robot's working zone, see Fig. 1.1. Nevertheless, if close interaction between human and robot is needed, a new solution must be used to reduce risk.

Efforts have been done by International Organization for Standardization (ISO) and American National Standards Institute (ANSI) regarding safety with robotized processes, where design recommendations include physical barriers equipped with sensors, clearance distance around the working area, remote robot's state diagnostic , proper illumination, workers training and process supervision [7]. ANSI/RIA R15.06-1999 is a standard for robot safety in factories, addressing the requirements for personnel safety in industrial environments where robotic manipulators are employed; however, there are no specifications for the case when robots and people have to share the operational space [8]. ISO-1028-1 and ISO-1028-2 are international standards that account safety requirements for

robots and robotic devices in an industrial environment, providing guidance in hazard recognition, and recommendations in design, manufacturing, installation, operation, maintenance and decommissioning of the industrial robot system or cell. It is worth to note that the sources of hazards are frequently unique to a particular robot system, directly related to the nature of the automation process and the complexity of the installation. The risks vary with the type of robot used, its installation, programming, operation and maintenance [9, 10].

1.1.1 Human-robot interaction (HRI)

The interest of moving robots from factories to human environments is growing due to the elderly population in developed nations, the desire of automatizing common daily tasks, and the lack or high cost of local human expertise [11]. A collaborative situation is when humans and robots are working in the same space at the same time [5]. ISO defined a Cooperative robot (cobot) as "a robot designed for direct interaction with a human". Depending on the application area, a cobot could be industrial, professional, or personal service robot [12].

Cobots must combine dexterity, flexibility and problem-solving skills of human workers with the strength, endurance and precision [13], see Fig. 1.2. Cognitive interactions between a robot and a human worker (cHRI) can lead to mental health risks for the human worker if not handled properly [14]. Here, the information exchange between human workers and robots flows in both directions, and is on an equal level of importance with regard to work processes [12].

Collisions occurring between the robot and its user are a very important topic in HRI. Severity indices of injuries are used to evaluate the safety in physical human-robot interaction (pHRI). These should take into account the possible damages occurring where a robot collides with a human [11].

Personal care robots are low power and not very precise cobots [16], like the ones shown in Fig. 1.3. They come in contact with a wide range of inexperienced people with robotics, like children and elderly, who may not be able to understand and react in an appropriate way to hazardous situations. Thus an approach to guarantee safety independently from the users' experience and actions is required for the new service robot domains [17].

Figure 1.2: YuMi-IRB 14000 industrial cobot. Its "inherently safe" design, allows it to work alongside humans while reducing risks to acceptable safety levels [15]

ISO-13482 defines requirements for design and safety validation of the intended robot's contact, taking into account the type of contact between robot and human, and where on the human body the contact is made. The products and devices that are currently on the market are not able to fully meet all of the requirements expected of safe and unhindered human-robot collaboration today. The development of new sensor and robot technologies, along with intelligent

(a) Care-O-bot 4

(b) Pepper

Figure 1.3: Personal care robots. Care-O-bot 4 is a modular mobile robot assistant to actively support humans in domestic environments developed by Fraunhofer Institute for Manufacturing Engineering and Automation [18]. Pepper is a social humanoid robot able to recognize faces and basic human emotions developed by Softbank Robotics. It is optimized for human interaction and is able to engage with people through conversation and his touch screen [19]

control systems, is a fundamental requirement for future collaborative robot applications [5].

1.2 Variable stiffness actuators

Mechanical design of machines is important for improving safety and performance. Some design applications for this end are: (*i*) the elimination of pinch points and sharp edges can reduce the potential for laceration or abrasion injuries, (*ii*) careful and light-weight design of moving parts, (*iii*) and introduction of compliance on purpose can reduce the effects of impacting loads in case of collisions [20].

Compliant transmissions ensure safe interaction but are inefficient in transferring energy from actuators to the links. An approach to increase performance for safe joint actuation is to allow the passive compliance of transmission to vary during the task's execution. Variable impedance actuator (VIA) is a mechanical/control co-design that allows changing efficiently the value of mechanical components such as stiffness, damping, and gear-ratio, guaranteeing low levels of injury risk and minimizing negative effects on control performance. For a mechanism with given total inertia and actuator limits, it is possible to formulate an optimal control problem to be used for comparing mechanical actuation alternatives at their best control performance. One known example is the safe Brachistochrone formulation, that proposes finding the minimum time necessary to move between two given configurations, such that an unexpected impact at any instant during motion produces an injury severity index below a given safety level. Its optimal solution obtained analytically and numerically shows that low stiffness is required at high speed [11].

Depending on how the desired stiffness and damping characteristics are achieved, VIAs are categorized into: (*i*) active impedance by control, (*ii*) inherent compliance, (*iii*) inherent damping, and (*iv*) inertial. Passive or fixed compliance actuators (PCA), active compliance actuators (ACA), and VSA belong to the second category.

PCAs, composed of stiff actuation and elastic elements to store energy, are characterized by the inability to control the natural frequency of a mechanical

system. ACAs use stiff actuators to adapt the stiffness of the system by software control, which implies having a closed loop system that uses sensors to measure position and relevant quantities, such as output force. Their main disadvantage is the continuous energy dissipation. Based on the previous concepts, VSAs are designed to combine energy storage and adaptable stiffness [1, 4, 21–23].

The applications that require controllable stiffness can be identified as *robot-human interaction* and *natural dynamics adjustment* [4]. The first one is focused on having a safer and more natural interaction between the human and the machine, some examples are industrial robots [2, 24–26] and human rehabilitation devices [27], while the second one deals with the adjustment of natural dynamics of the mechanical system in order to have a desired natural motion to reduce the energy consumption: robotic prosthesis [28, 29] and legged robots [30] are the most notable examples.

Several types of VSA have been developed, the majority use mechanical springs and other elastic elements along with motors to obtain the desired position [2]. These actuators adapt the stiffness based on sensory feedbacks. The effectiveness of this approach is limited by the bandwidth of the system [31,32], which is mainly driven by the response time of the controller that is using information from the sensors. Pneumatic actuators have been used to achieve variable stiffness in robotic devices. The approach presented in [33] considers the dynamic characteristics of a pneumatic cylinder as a series elastic actuator, by replacing a four-way servo valve with a couple of three-way valves, which allows the user to modulate the stiffness and the output force. Spring over muscle actuators (SOM) are composed of pneumatic muscles attached in parallel with standard compression springs in a cylinder-plunger arrangement; their are utilized to actuate gait trainer for ankle rehabilitation [34]. Variable stiffness device (VSD) units with nonlinear stiffness characteristics were developed to adjust the compliance of cable-driven manipulators in [35,36]. The total stiffness is given from cable stiffness and VSD by attaching a VSD along each cable of the manipulator in a serial manner. Robot's stiffness can thus be controlled by manipulating cable tensions.

The idea of biphasic media used for variable stiffness actuation has been studied in [2, 27, 31, 32]. The models were designed using pneumatic and hydraulic components. The gas fraction works as nonlinear elastic element, providing varia-

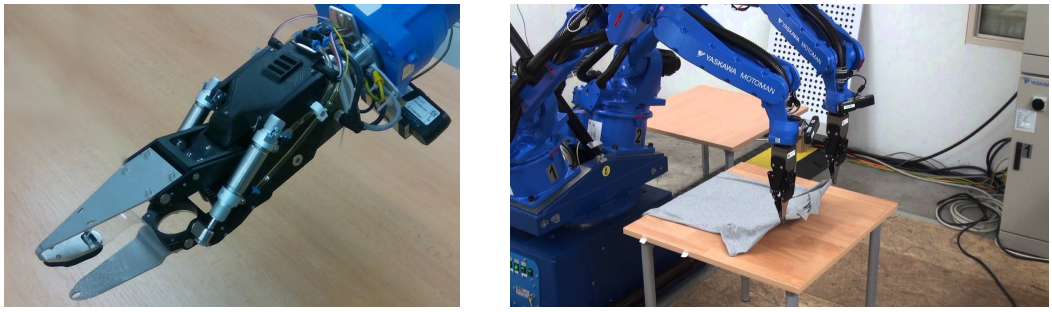

(a) CloPeMa gripper **(b)** Manipulation and identification task

Figure 1.4: Clothes Perception and Manipulation (CloPeMa) gripper uses BMVSA technology in order to manipulate and identify different apparels

tion of stiffness of the system due to pressure gas changes, while the liquid one is assumed incompressible and used to provide pressure changes and motion to the output link. The major implementations of the system are industrial grippers for garment handling, see Fig. 1.4, and surgical robotics concepts.

1.2.1 VSA classifications

A VSAs' classification according to the mode to achieve adjustable compliance is given in [4] and shortly described next.

1. **Equilibrium-controlled stiffness.** They use a fixed stiffness spring in series with a traditional method of actuation (motors, hydraulic actuators). To obtain variable stiffness, the virtual stiffness is adjusted by dynamically adjusting the equilibrium position of the spring [37,38]. Series elastic actuator (SEA) has been exhaustively studied and implemented for bionic ankles and humanoid actuation [39], like the one shown in Fig. 1.5b.

2. **Antagonistic-controlled stiffness.** Two actuators with non-adaptable compliance and nonlinear force-displacement characteristics are couple antagonistically using nonlinear springs, see Fig. 1.6. To change stiffness, it is required a linear resulting spring characteristic of the setup, as shown in section 1.2.2. The most known example of an antagonistic setup is the combination of muscles composing biceps and triceps, hence, this approach

is called *biologically inspired*. A simple and efficient application of this approach is described in [40], consisting of two nonlinear SEA attached to a rotational joint. The actuator with mechanically adjustable series compliance (AMASC) [41] is able to control compliance and equilibrium position independently thanks to the smart arrangement of pulleys, rendering an easier controller for the system. Designs using pneumatic components are often used when a high power-to-weight ratio is required, the most known are Pneumatic artificial muscles (PAM)s and pleated PAM [42, 43].

3. **Structure-controlled stiffness.** This approach is characterized by modulating the effective physical structure of a spring to achieve variations in the stiffness, like material modulus, moment of inertia and effective beam length. The jack spring actuator, using helical springs, is an example of this concept; its working principle is adjustment of compliance by adding or subtracting the number of available coils used in the spring [44].

4. **Mechanically controlled stiffness.** Changing the pretension or preload of the spring allows these devices to adjust compliance. These actuators behave as torsion springs with independent controllable spring characteristics and equilibrium position. One method used in this approach is the lever arm length adjustment, where the variation of compliance is based in the change of lever's length using only one passive element [4]. The mechanically adjustable compliance and controllable equilibrium position actuator (MACCEPA) was designed based on the previous method. The control of compliance and equilibrium position are independent from each other and the current position of the actuator [45].

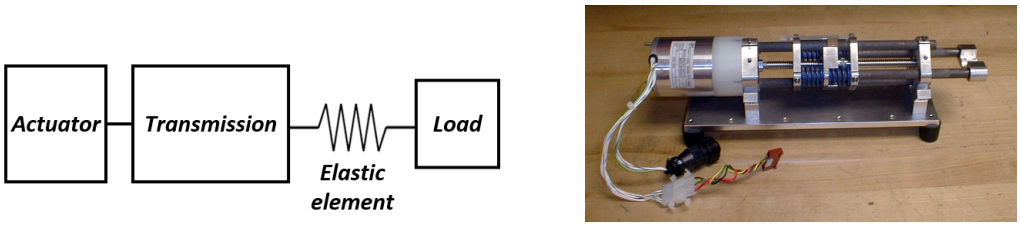

(a) SEA schematic **(b)** MIT's SEA device used in M2 project

Figure 1.5: Equilibrium-controlled stiffness actuators

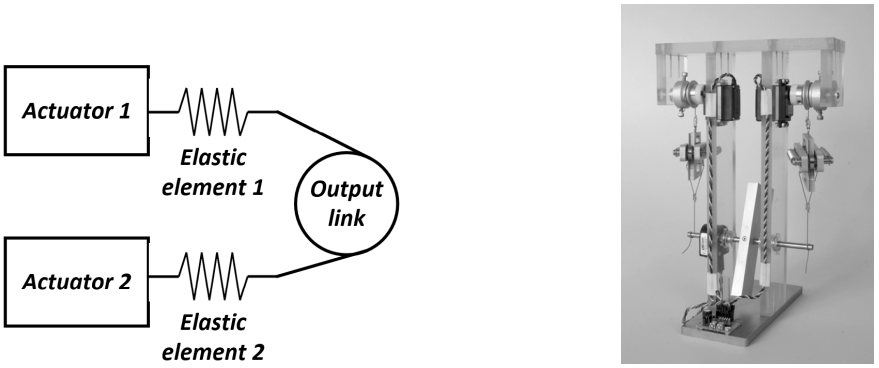

(a) Antagonistic setup schematic **(b)** Migliore's quadratic spring device

Figure 1.6: Antagonistic-controlled stiffness actuators

1.2.2 Nonlinear springs for antagonistic setups

Based on the simple linear antagonistic setup displayed in Fig. 1.7, a demonstration showing the necessity of using a couple of nonlinear springs for controlling the stiffness of the system is developed [4]. The selected springs are linear and have the same spring constant ($k_1 = k_2 = k$). x_{0A} and x_{0B} represent the controllable positions of blocks A and B when the rest lengths of both springs are zero. These positions can be adjusted independently by using two actuators. The force applied on the cart is given in 1.1, while the stiffness (K) is defined in 1.2.

$$F = -k(x - x_{0A}) + k(x_{0B} - x) = -2kx + k(x_{0A} - x_{0B}) \tag{1.1}$$

$$K = \frac{dF}{dx} = -2k \tag{1.2}$$

K is uncontrollable if linear springs are chosen, because it is independent of x_{0A} and x_{0B}. When nonlinear springs are used, the force on the cart is no longer linear, consequently, rendering a stiffness that is affected by the controllable positions.

1.3 Thesis contributions

The goal of this project is to develop and test a variable stiffness actuator using biphasic media technology. This type of VSA is expected to replace normal

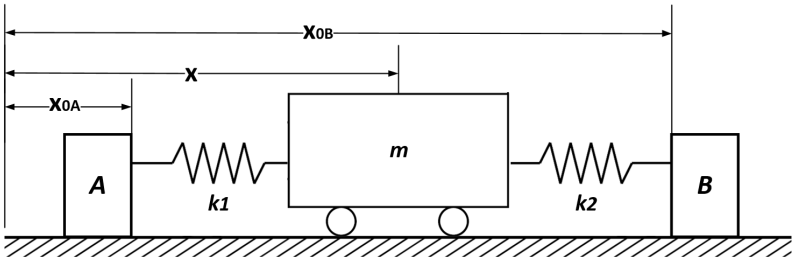

Figure 1.7: Antagonistic VSA setup demonstration of need for nonlinear springs

hydraulic cylinders in different machines in order to improve safety and comfort. The detailed contributions of this thesis are:

1. Modeling the BMVSA as a damped harmonic oscillator and controlling its position and stiffness with a model-based approach.

2. A previously manufactured prototype of the BMVSA was studied, modified and tested. Later, this device was mounted on a revolute joint mechanism with one degree of freedom (DOF) in order to analyze its performance.

3. To extend the BMVSA applications, actuator-level collision event algorithms were simulated and implemented in the prototype.

4. Applications using cables combined with this technology were proposed and formulated.

1.4 Outline

The development of BMVSA system was taken as a leveled project, where mathematical modeling was based on mechanical design. It is worth to note that each chapter contains relevant content that has been already accepted for publications and oral presentations in international events. This thesis is organized as follows.

Chapter 2: This chapter details the design, characteristics and modeling of biphasic media variable stiffness actuation. It also provides a wider view on design

and selection of the system's components.

Chapter 3: This section discusses the possibility of using a model-based position and stiffness controller for the system. Equations defining the controller are developed and simulation's results analyzed.

Chapter 4: This episode studies a prototype and a testing mechanism. The design elements of the prototype are listed and the corresponding equations that describe the workbench are provided.

Chapter 5: This section presents an introduction to algorithms used in collision events involving BMVSAs. The algorithms cover different sections of the collision pipeline, including detection, classification and reaction.

Chapter 6: An introduction for applications related to cable-actuation using BMVSA is provided. Simulations of a single dof joint mechanism proved the feasibility of the system.

Chapter 7: Finally, this section summarizes the results observed during the development of this project. The description of the ongoing work is given with a possible future research direction.

Appendix A: This is a short chapter that deepens in the physical characteristics of the actuator, like friction in hydraulic cylinders.

Appendix B: This annex provides the description of the components used in the prototype and mechanism.

Appendix C: Publications related to this thesis are briefly reported.

Chapter 2

Biphasic media variable stiffness actuation

Biphasic media variable stiffness actuators are designed using pneumatic and hydraulic components. A control fluid must be used in order to transmit motion into the circuit. This fluid is composed of two non-mixable fluids with different coefficients of compressibility, disregarding their phase (liquid or gas). In order to increase the variation of compliance, a combination of gas and liquid is preferred. The gas works as nonlinear elastic element, altering the stiffness due to pressure gas variations, while the liquid is assumed incompressible and used to provide pressure changes and motion to the output link. Fig. 2.1 represents the primal embodiment of this approach, where confined gas fractions are dispersed in the liquid. In this system, force applied to the environment depends on pressure difference between the distribution lines. Sensors are used to measure pressures and piston's position. It is worth mentioning that it is preferable that the gas is close to surface of the output link of the actuator, since the volume of liquid involved when an external force moves the output link and changes the pressures of the gas fractions is minimum [32]. In event of collision, the pressure in one of the lines increases, leading to compression of gas in the chamber, which thresholds the actuation force applied to the driven link by the actuator and the inertial force applied to the driven link through the actuator by the preceding link [2].

Based on the notations of Fig. 2.1, the actuator is composed of a double

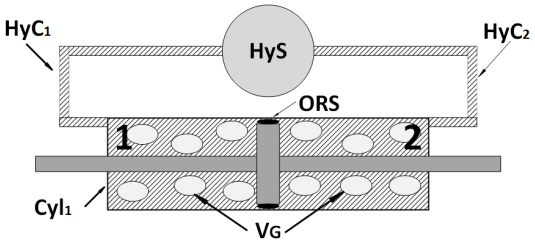

Figure 2.1: Original embodiment of BMVSA

acting hydraulic cylinder *(Cyl1)* connected to a hydraulic circuit, inside which a control fluid circulates. The hydraulic circuit includes a supply and distribution system *(HyS)*. The circuit has two hydraulic distribution lines (*HyC1* and *HyC2*) respectively connected to the cylinder's chambers (1 and 2). The control fluid encompasses two different fluids in predefined proportions; in this case, liquid (mineral oil) and gas (Nitrogen (N)), having the compressible fluid dispersed in the chambers and considered as a total volume (VG). O-ring type seals *(ORS)* provide the translation of the piston without leakage. The hydraulic circuit must include elements that vary pressure inside the chambers with aim of controlling stiffness of the actuator, like pumps and valves.

Considering a displacement of the piston compressing the fluid contained in chamber 1, in such a way that it behaves as the suction chamber, while chamber 2 acts as the discharge one. The system will follow one of the three following modes:

1. VG remains constant, the fluid flowing respectively inside/outside chambers is the same, and the piston moves at constant velocity, while the stiffness of the system is constant.

2. VG decreases, the fluid entering in chamber 2 is higher than the volume leaving chamber 1, and the stiffness of the system increases.

3. VG increases, the fluid entering in chamber 2 is lower than the volume leaving chamber 1, and the stiffness of the system decreases.

The system can be driven back to mode 1 after the stiffness has reached the desired value.

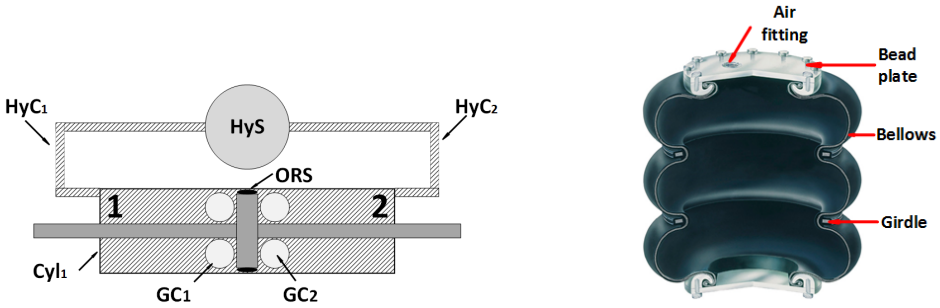

(a) Pneumatic containers BMVSA approach **(b)** Typical air spring

Figure 2.2: BMVSA using pneumatic containers as compliant component

2.1 BMVSA architectures

The introduction of a compressible fluid into the system can be done in different ways, knowing that the fluids should not be miscible. Figure 2.2a displays an approach characterized by keeping the compressible fluid (N) inside sealed elastic containers, shown as GC_1 and GC_2. These containers must be distributed inside the cylinder's chambers in a logic proportion, which adds a degree of complexity for the generation of the embodiment. One important feature is the relative fixed equilibrium position of the system when the circuit is open due to the fact that the containers occupy some part of the chambers' volumes. Pneumatic or air springs are devices that might serve for this purpose; they contain a column of air in an elastomeric bellow or sleeve, see Fig. 2.2b. They are commonly found in vehicle suspension systems, occasionally in conjunction with a coil spring, they are also used to insulate vibration in machinery and as linear or angular actuators [46].

Figure 2.3a is a design that shares the functioning principle of the hydropneumatic suspension (HPS) [47, 48]. It is convenient due to its modularity, where the gas fraction is contained in hydropneumatic accumulator (HPA) that can be easily connected to the circuit and substituted if different gas characteristics are needed. The equilibrium position of the system is variable when the circuit is open because of HPA's volumes are not affecting the volume of the cylinder. The amount, size, distribution, type, and precharge of the HPA are design parameters that directly affects the stiffness of the system. Figure 2.3b displays a diaphragm type HPA defined by the use of a elastic diaphragm as separation membrane between the

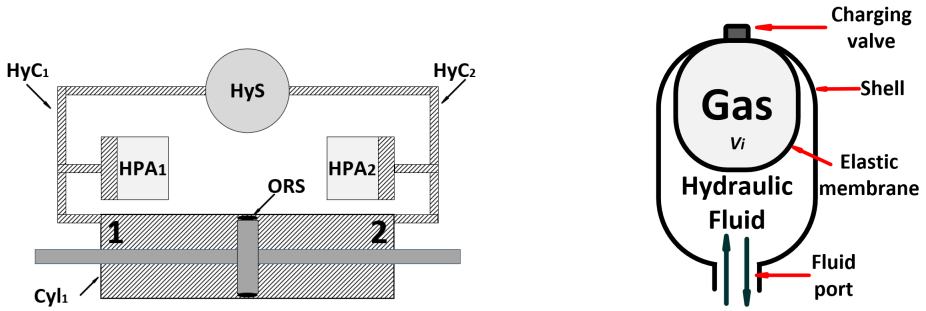

(a) HPA-BMVSA **(b)** Hydropneumatic accumulator schematic

Figure 2.3: BMVSA using hydropneumatic accumulators as compliant component

fluids.

2.1.1 Hydropneumatic suspension principle

A basic HPS system consists of a hydraulic cylinder, a HPA, a control fluid, and a position control unit, as shown in Fig. 2.4. Additional oil lines and fittings are necessary if the cylinder and accumulator need to be separated. In the case of additional damping, a flow resistor can be placed between cylinder and accumulator, converting some kinetic energy of the oil into heat. The control unit provides a constant normal position of the suspension independent from the static spring load. This unit consists of a position sensor and a pressure gauge connected to a hydraulic control valve, which is able to change the amount of oil in the circuit.

The stiffness of the suspension can be modeled taking into account the initial and final state of this system. Let F be an external force acting upon the piston rod in balance with the resulting force from HPA's pressure P_A acting on the piston's area (A), while neglecting inertial and friction forces. If the force F is increased to F^*, the position of the piston changes ($\Delta x = x - x^*$) and therefore some liquid moves into the accumulator. This change continues until the pressure in HPA reaches a value that provides a balance for the system (P_A^*), as shown in (2.1). The spring stiffness k_s is defined as the difference of forces in the initial and

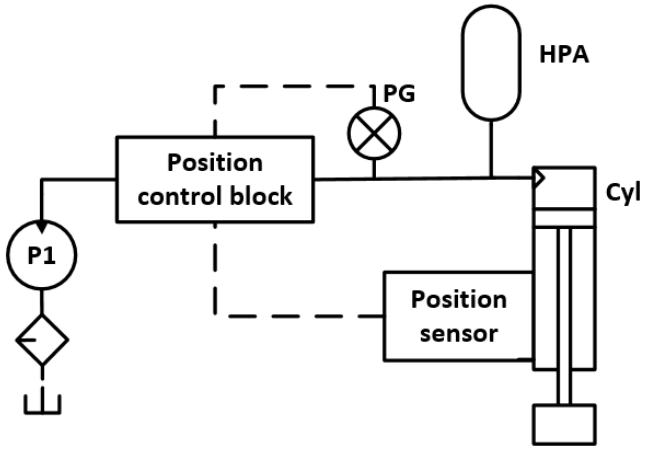

Figure 2.4: Basic setup of a hydropneumatic suspension

final state with respect to the piston's displacement, like displayed in (2.2).

$$\begin{aligned} F &= P_A A \\ F^* &= P_A^* A \end{aligned} \tag{2.1}$$

$$k_s = \frac{F - F^*}{\Delta x} \tag{2.2}$$

A change in pressure in the system causes a variation in the position. The most notable physical reasons and their stiffness constants are: *(i)* compression of the gas HPA (k_G), *(ii)* widening of the elastic fluid lines and fittings (k_L), and *(iii)* compression of the hydraulic fluid (k_H). The suspension spring rate is sequential combination of these three individual springs, as shown in (2.3) .

$$k_{HPS} = \frac{k_G k_L k_H}{k_G k_L + k_G k_H + k_H k_L} \tag{2.3}$$

k_L and k_H are usually high compared with k_G, so their impact on the overall spring rate is low, meaning that HPS stiffness is mainly influenced by the properties of the gas contained in HPA.

2.1.2 Hydropneumatic accumulators

Accumulators are installed in hydraulic systems to store energy and to smooth out pulsations [49]. They are also used to supply emergency power for braking and steering systems [50, 51]. There are three principal types of accumulators, each has particular advantages as well as limitations which should all be considered when selecting an accumulator for a specific application, see to Fig. 2.5.

- Bladder accumulator has a flexible bladder as a separation element between compressible gas cushion and operating fluid. It consist of a welded or forged pressure vessel, the accumulator bladder and the fittings for the gas and fluid side connection.
- Piston accumulator encompasses a free-moving piston as a separation element between a compressible gas cushion and the operating fluid. It is comprised of a cylinder with screwed-in cover on the gas and fluid side as and a piston with special sealing systems. The piston position can be used for switching functions in the hydraulic system.
- Diaphragm accumulators contain a flexible diaphragm as a separation element between the compressible gas cushion and the operating fluid. It is designed either as welded or as cartridge constructions and offered in various different steels, elastomers and gas connections.

Bladder and diaphragm accumulators are preferred for applications requiring rapid cycling, resistance to high fluid contamination and fast response times.

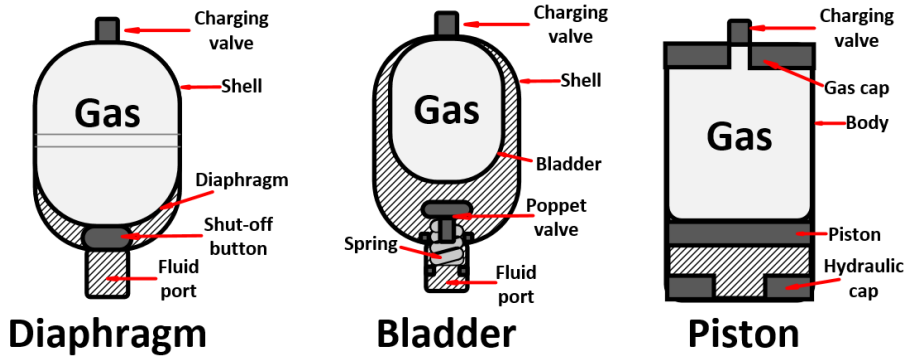

Figure 2.5: Hydropneumatic accumulators

Piston accumulators offer greater efficiency and flexibility in most applications due to their wider range of sizes.

HPAs incorporate a gas with a hydraulic fluid. The fluid has minimum dynamic power-storage qualities; typical hydraulic fluids can be reduced in volume by only about 1.7% under high pressure (more than 5000 psi). This characteristic makes them ideal for power transmission. On the other hand, gas can be compressed into small volumes at high pressures. Potential energy is stored in the compressed gas to be released upon demand [49].

2.2 Damping in hydraulic cylinders

The external energy applied onto the system is dissipated due to damping, creating a decay of the resulting oscillation amplitude. Boundary and fluid friction are fundamental principles that generate damping in the system. During the design process, damping forces are kept as low as possible to get the best possible decoupling of the suspended mass on the isolated side from the excitation on the input side. However, if the level of damping is tuned to provide optimal results under normal operating conditions, it could not work properly under extreme operating conditions. For these situations, additional damping elements, like throttle valves, are used to dissipate the excessive kinetic energy before piston reaches the end stop [48, 52]. To keep a simple modeling, the friction is taken as a viscous coefficient of friction (μ) proportional to the velocity of the system [53]. A deeper explanation regarding friction in hydraulic cylinders is given in Appendix A.

2.3 Modeling of BMVSA

In order to ease the modeling of the system, some assumptions regarding its thermodynamic characteristics must be taken: (i) the gas is considered ideal and immiscible with the fluid, (ii) there is no leakage from the HPAs, (iii) there is no leakage between the cylinder chambers, and (iv) the temperature is constant (isothermal transformations; if operating at high frequency, the actuator undergoes

adiabatic transients not considered). (2.4) defines these characteristics.

$$P_i v_i = n_i R T_i \tag{2.4}$$

where v_i is the volume of gas in the i^{th} HPA, n_i is the number of moles for its corresponding gas fractions, R is the ideal gas constant, and T_i is the temperature in the i^{th} chamber.

The BMVSA is described as a damped harmonic oscillator in (2.5), where m is the mass of the output link of the actuator, (piston, seals and mechanical attachments), x_p is the displacement of the piston, k_v is the coefficient of viscosity, F_p is the force generated by the difference of pressures P_1 and P_2 acting on the piston's head surface S, as shown in (2.6), and F is an external force. From (2.5), it can be stated that F_p is taken as the restoring force of the system. The subscripts 1 and 2 denote chambers 1 and 2 and their corresponding HPAs.

$$m\ddot{x}_p + k_v \dot{x}_p - F_p = F \tag{2.5}$$

$$F_p = (P_1 - P_2)\, S \tag{2.6}$$

Considering an uniform temperature in the whole system, (2.7) can relate pressures and volumes.

$$P_i v_i = C_i \tag{2.7}$$

and C_i is the gas constant, which can be considered equal for both sides if the HPAs have the same characteristics ($C_i = C_1 = C_2$). In (A.2), the volumes are expressed as the sum of added oil volumes into the hydraulic circuit (v_{ai}) and the oil coming from the cylinder (Sx_p).

$$\begin{aligned} v_1 &= v_1(0) - v_{a1} - Sx_p \\ v_2 &= v_2(0) - v_{a2} + Sx_p \end{aligned} \tag{2.8}$$

The instantaneous stiffness K is the derivative of force generated by the difference of pressures in the cylinder with respect to displacement. Equation (2.9) shows that stiffness is a function of v_{ai}. If fluid is added to both chambers, the

volumes of gas reduce and the pressures increase. Similarly, if fluid is subtracted from both chambers, the volume of gas increases and the pressure in both chambers reduces.

$$K = \frac{\partial F_p}{\partial x_p} = CS^2 \left(\frac{1}{v_1^2} + \frac{1}{v_2^2} \right) \tag{2.9}$$

When no external force is applied onto the system, the damped harmonic oscillator can be described by the equation below.

$$\frac{d^2x}{dt^2} + 2\zeta\omega_0 \frac{dx}{dt} + {\omega_0}^2 x = 0 \tag{2.10}$$

where ω_0 is the undamped angular frequency, and ζ is the damping ratio.

$$\omega_0 = \sqrt{\frac{K}{m}} \tag{2.11}$$

$$\zeta = \frac{k_v}{2\sqrt{mK}} \tag{2.12}$$

This is system is designed to be underdamped ($\zeta < 1$), meaning that the system oscillates with the amplitude gradually decreasing to zero. The angular frequency is given in (2.13), and the exponential decay is given by (2.14).

$$\omega_1 = \omega_0 \sqrt{1 - \zeta^2} \tag{2.13}$$

$$\lambda_e = \omega_0 \zeta \tag{2.14}$$

In terms of energy, when a spring is stretched or compressed, it stores elastic potential energy (E_P), which then is transferred into kinetic energy (E_k), this analogy helps to understand how the energy is kept in the compressed gas of the BMVSA [54–56]. E_P within a spring is determined by the equation (2.15), while E_k is defined in (2.16).

$$E_P = kx^2/2 \tag{2.15}$$

$$E_k = \frac{1}{2} m \dot{x}^2 \tag{2.16}$$

By conservation of energy, assuming the system is at the equilibrium position, when the spring reaches its maximal E_P, the kinetic energy of the mass is zero. When the spring is released, it tries to return to equilibrium, turning its E_P into E_k. This is an important study to take into account regarding improvements in energy efficiency in the system.

2.3.1 Design considerations

In order to design a device that behaves according to specifications, the following design considerations must be accounted [48].

- Optimal selection of sealing elements, seal geometry and the seal material, must be performed in the beginning of the system layout. In particular the seal diameters have a great influence: the larger the seal diameter, the longer the length of the sealing edges and the higher the friction forces.

- Precharge of HPA. Correct precharge involves accurately filling an accumulator's gas side with a dry inert gas, while no hydraulic fluid is in the fluid side. Charging then begins when hydraulic fluid is admitted into the fluid side, and occurs only at a pressure greater than the precharge pressure. During charging, the gas is compressed to store energy. The care with which precharging must be accomplished and maintained is an important consideration when choosing the type of accumulator for an application, all else being equal. If the wrong accumulator was selected, premature failure is almost certain.

- Dimensioning of components. This is determined by the hydraulic pressure of the system. Depending on the pressure level, the elements need to have the correct dimensions to provide the right amount of active area and to provide enough mechanical stability to withstand inner pressure loads. It is essential to consider that dynamic pressure variations add to the pressure in static state(design position). Some factors are: (i) amount of hydraulic fluid

that is exchanged between cylinder and accumulator, and (*ii*) the kind of operation of the accumulator (gas volume at static pressure).

- Dimensioning and type of hydraulic cylinder. The piston diameter is determined by trying to make the maximum use of the available system pressure. Rod diameter and cylinder stroke are the defining parameters for a cylinder which are completely dependent on the type of external system's load and task.

- Selection and positioning of hydraulic lines and fittings. These elements enable the connections of the components according to the hydraulic schematic. The circuit lines are important since the hydraulic fluid in the lines is in permanent motion and their flow restriction effect has a direct influence on the system's behavior. Due to the high flow rates, the diameter of these lines should be chosen to be as large as possible. Since the fluid guiding elements have throttle-type flow resistance, their influence on damping is very strongly dependent on fluid viscosity and temperature. So it is especially important for suspension systems in applications with low operating temperatures to pay special attention to low flow resistance of the lines.

Chapter 3

Position and stiffness control of BMVSA

This chapter focuses on the development of a model-based control method to track the desired position and stiffness. Firstly, a short review of the previously implemented control approaches are given: Proportional Integral Derivative (PID) and Fuzzy. Later on, the mathematical model of the controller is proposed. Finally, results from force loaded and unloaded simulations and possible applications of the system are discussed.

3.1 Position and stiffness control approaches

Based on equations (2.5), (2.6), and (2.7), it is possible to design a control strategy able to manipulate the position and the stiffness of the system at the same time. The usual method to control position in a hydraulic cylinder is performed by controlling the pressures in both chambers, hence, movement is done whenever the pressures are different. The approach for the stiffness is similar but it is related to the amount of pressure in each chamber: the higher the pressure, the higher the stiffness, and vice versa. The sensors used to obtained the feedback are encoders for position and pressure gauges for the cylinder chambers. In general, the errors in position and stiffness must be minimized during the process.

3.1.1 Dual coupled PID controller

In [32], a couple of PID controllers was used to control stiffness and position. Flows q_1 and q_2 are the control variables. The measured quantities are the position of the piston (x_p) and the pressures in the two chambers (P_i). The pressures are used to calculate the current stiffness (K) using (2.9). Knowing that the position depends on $q_1 - q_2$ and the stiffness on $q_1 + q_2$, two PID controllers relate the flows q_1 and q_2 to the position error e_x and stiffness error e_K.

$$\begin{aligned} q_1 - q_2 &= k_{px} e_x + k_{dx} \frac{de_x}{dt} + k_{ix} \int_0^t e_x dt \\ q_1 + q_2 &= k_{pK} e_K + k_{dK} \frac{de_K}{dt} + k_{iK} \int_0^t e_K dt \end{aligned} \tag{3.1}$$

where k_{px}, k_{dx}, and k_{ix} are the proportional, derivative and integral gains used in the position controller; k_{pK}, k_{dK}, and k_{iK} are the proportional, derivative and integral gains used in the stiffness controller. The gains were tuned heuristically through simulations. The schematic of the system is shown in Fig. 3.1. The results from this approach suggest that a more sophisticated control architecture is necessary to exploit the whole range of stiffness variation available.

3.1.2 Fuzzy controller

Fuzzy control is a practical alternative for a variety of challenging control applications since it provides a convenient method for constructing nonlinear controllers via the use of heuristic information. This controller works as an artificial decision

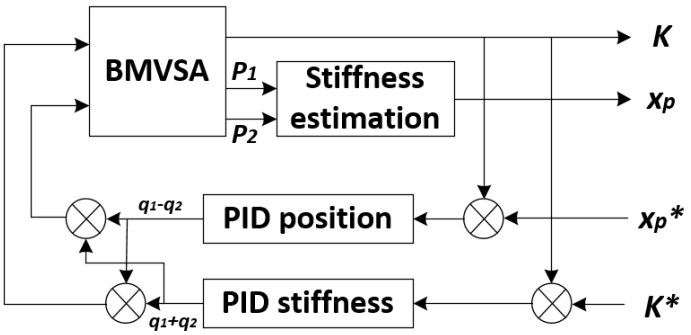

Figure 3.1: Dual PID controller schematic

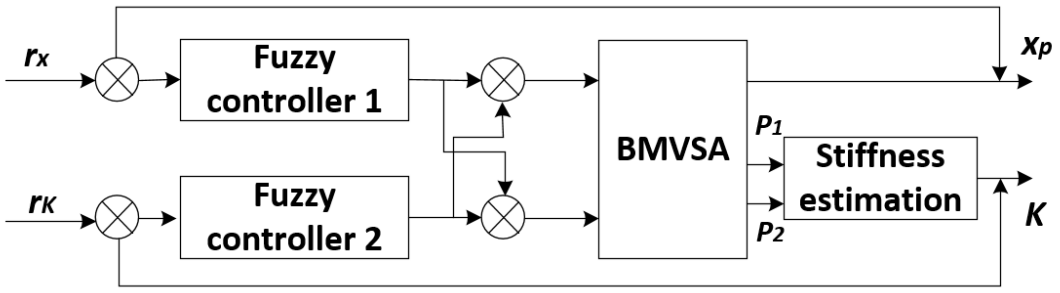

Figure 3.2: Adaptive fuzzy controller schematic

maker that operates in a closed-loop system in real time. It gathers plant output data $y(t)$, compares it to the reference input $r(t)$, and then decides what the plant input $u(t)$ should be to ensure that the performance objectives will be met. The adaptive fuzzy control, implemented in [32], consists of two parts: the conventional PID controller, and the fuzzy controller. A two inputs and three outputs fuzzy adaptive PID controller was designed with the objective is to find the fuzzy relations among K_p, K_i , K_d, and error rate, as shown in 3.2. The simulation results show that the fuzzy adaptive PID controller has better stability, small overshoot, fast response.

3.1.3 Model-based controller

Model-based tracking for nonlinear systems is a part of control where tracking is goal and a controller is based upon a dynamic model [57]. Model-based control outperforms kinematic-based control with regard to performance, control precision, ability to cope with external disturbances, friction, and noise. The first step in this technology is the development of a custom physics-based computer model of the system to be controlled. The model is then validated using experimental data from the system or simulations.

The functional characteristics of the actuator depend on its design and the initial conditions. The measured quantities in the system are: *(i)* the position of the piston, and *(ii)* the pressures in the chambers. Equations (3.2) describe the volumetric flow rate, where q_i represents the moving volume in the system's chambers ($\dot{v_{ai}} = q_i$). At any instant, the volume subtracted or added fluid cannot

be larger than the total volume of gas since the liquid fraction is considered incompressible.

$$\begin{aligned} \dot{v_1} &= -q_1 - S\dot{x_p} \\ \dot{v_2} &= -q_2 + S\dot{x_p} \end{aligned} \tag{3.2}$$

Equation (3.3) was deduced considering u as spring's restoring force equal to F_p and x_p^* as the desired position, where K_E is the characteristic gain of the spring and u^* is the desired control signal. The error of position is stated in (3.4) and its derivative with respect to time in (3.5), where γ is the tuning parameter to achieve minimal error.

$$u^* = -K_E(x_p - x_p^*) \tag{3.3}$$

$$e = u - u^* \tag{3.4}$$

$$\dot{e} = \dot{F}_p - \dot{u^*} = -\gamma e \tag{3.5}$$

From the combination of (2.6) and (3.5) it is possible to write:

$$\dot{e} = \frac{S}{C}\left[{P_2}^2\dot{v_2} - {P_1}^2\dot{v_1}\right] - \dot{u^*} \tag{3.6}$$

Substituting (3.2) into (3.6) leads to:

$$\dot{e} = \frac{S}{C}\left[{P_1}^2 q_1 - {P_2}^2 q_2\right] - w_{xp}(t) \tag{3.7}$$

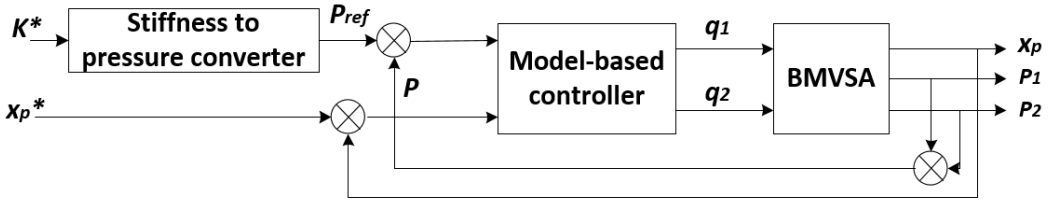

Figure 3.3: Model-based controller schematic

$$w_{xp}(t) = -\frac{S^2 \dot{x_p}}{C}\left({P_1}^2 + {P_2}^2\right) + \dot{u}^* \tag{3.8}$$

From substituting (3.5) into (3.7), the equation that controls the position of the system is obtained (3.9).

$$\begin{aligned} b_{xp}(t) &= {P_1}^2 q_1 - {P_2}^2 q_2 \\ b_{xp}(t) &= \frac{C}{S}\left(-\gamma e + w_{xp}(t)\right) \end{aligned} \tag{3.9}$$

Based on equation (2.9), it is possible to confirm that the direct relation between pressures and stiffness of the systems allows controlling the stiffness of the system. The pressure control equations were developed following the previous procedure used for position control. The error of pressure is used to control the stiffness, which is defined as the difference between the current pressures of the system and the ones related to desired stiffness (P_{ref}), as shown in (3.10).

$$e_p = \left(\frac{P_1 + P_2}{2} - P_{\text{ref}}\right) \tag{3.10}$$

Differentiating (3.10) with respect to time and substituting (3.2) leads to:

$$\dot{e_p} = \left(\frac{1}{2C}\right)\left((P_1)^2 q_1 + (P_2)^2 q_2\right) + w_p(t) \tag{3.11}$$

$$w_p(t) = \frac{S^2 \dot{x_p}}{2C}\left({P_1}^2 + {P_2}^2\right) - \dot{P}_{\text{ref}} \tag{3.12}$$

$\dot{e_p}$ is described in (3.13), where λ is the tuning parameter to achieve minimal error.

$$\dot{e_p} = -\lambda e_p \tag{3.13}$$

After substituting (3.11) into (3.13), the equation (3.14) is used to control the pressure.

$$b_p(t) = -2C\left(\lambda e_p + w_p(t)\right) \tag{3.14}$$

Expanding and solving (3.5) and (3.13) for q_i allows to control the position and

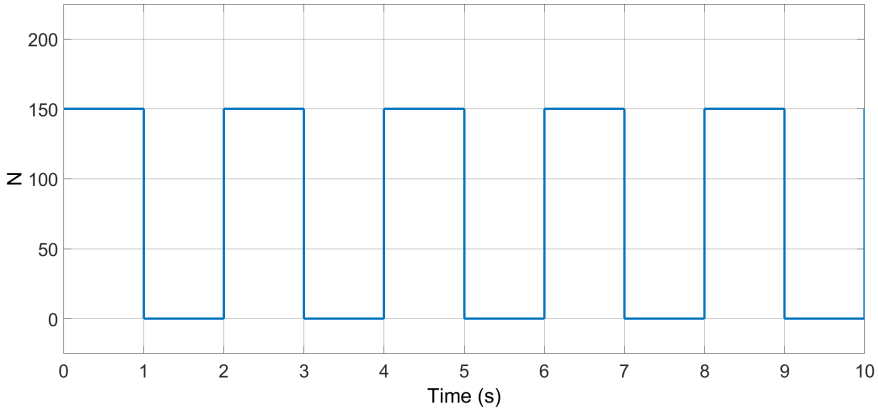

Figure 3.4: Load force signal

stiffness of the system as shown in (3.15), (3.16), (3.9), (3.14), (3.8) and (3.12).

$$\begin{bmatrix} q_1 \\ q_2 \end{bmatrix} = \begin{bmatrix} {P_1}^2 \\ -{P_2}^2 \end{bmatrix} Db_{xp}(t) + \begin{bmatrix} {P_1}^2 \\ {P_2}^2 \end{bmatrix} Db_p(t) \tag{3.15}$$

$$D = \frac{1}{{P_1}^4 + {P_2}^4} \tag{3.16}$$

The BMVSA can be considered to have antagonistic controlled stiffness [11], where two actuators with non-adaptable stiffness and nonlinear force-displacement characteristics are coupled antagonistically, working against each other. Based on the previous equations, an array of hydraulic proportional flow valves are used to the vary the pressures in both chambers.

3.2 Simulation

The following simulation was done to study the stiffness and position of the model using the parameters given in Table 3.1. Two types of tests were performed: the first did not have a load force applied, while the second one had a force signal with a square wave shape with 75 N amplitude and baseline on 75 N at 0.5 Hz, as shown in Fig. 3.4. Position in the actuator is measured from left of the cylinder to end to right end.

The desired position is given as a sinusoidal signal with 0.05 m amplitude

Table 3.1: Simulation parameters

Parameter	Value
m	$1\ Kg$
K_v	$0.5\ Ns/m$
K_E	$8x10^3\ N/m$
S	$3.776x10^{-4}\ m^2$
C	$300\ Pam^3$
γ	$-5x10^2$
λ	$-1.3x10^3$
$x_p(0)$	$0\ m$
x_pmax	$0.15\ m$
x_pmin	$0\ m$
$v_i(0)$	$1.5x10^{-4}\ m^3$

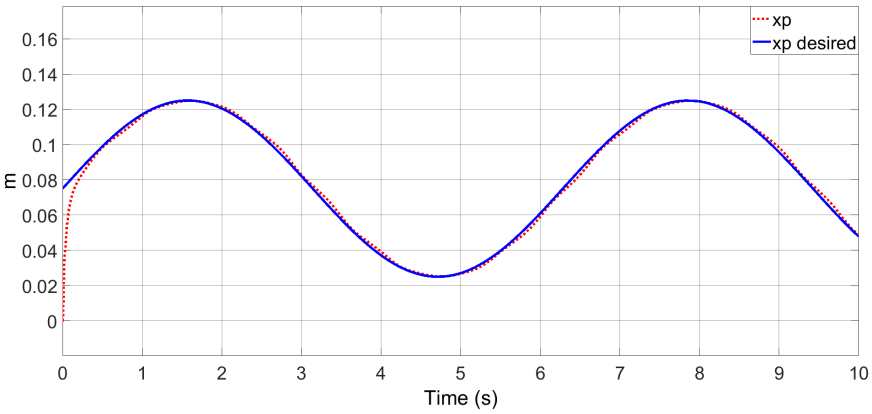

Figure 3.5: Position tracking during simulation

and baseline on 0.075 m at 0.16 Hz, while the desired stiffness is a sinusoidal signal with $2.5x10^4$ N/m amplitude and baseline on $5x10^4$ N/m at 1.6 Hz. The results of the simulations prove that the model-based controller is able to properly track position and stiffness even if the desired signals to follow are nonlinear as illustrated in Figs. 3.5, 3.6, 3.7 and 3.8. It is worth to note that the controller was tuned to prioritize stiffness tracking over position tracking as displayed in Fig. 3.6 and 3.8, whenever the load force differs from zero a displacement in the position of the actuator is generated. This displacement is directly related to the value of K_E.

Figs. 3.9 and 3.10 display the behavior of the volumes of gas inside the HPA.

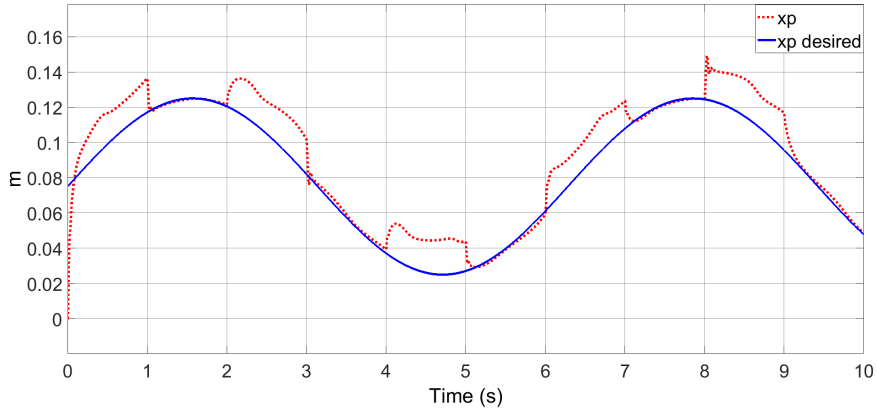

Figure 3.6: Position tracking during simulation with load force applied

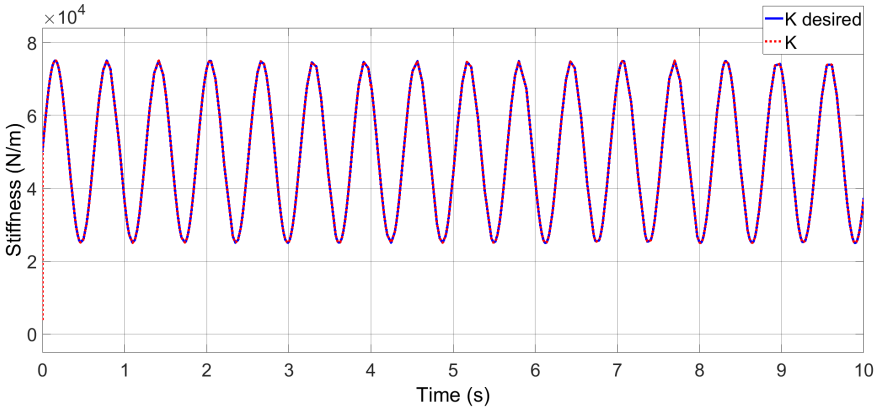

Figure 3.7: Stiffness tracking during simulation

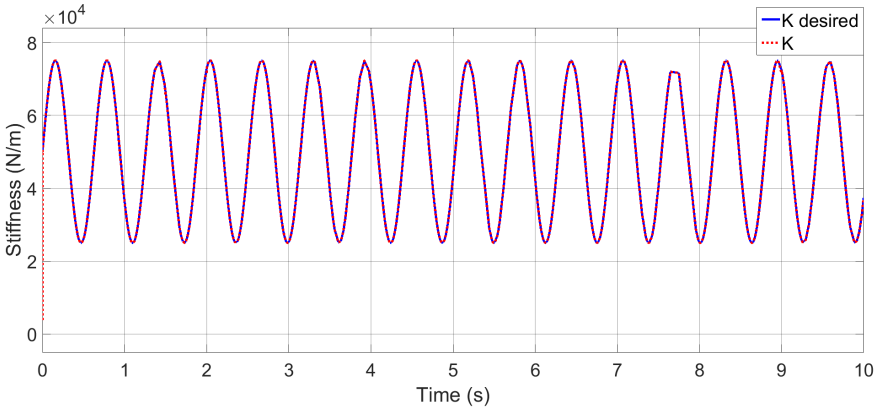

Figure 3.8: Stiffness tracking during simulation with load force applied

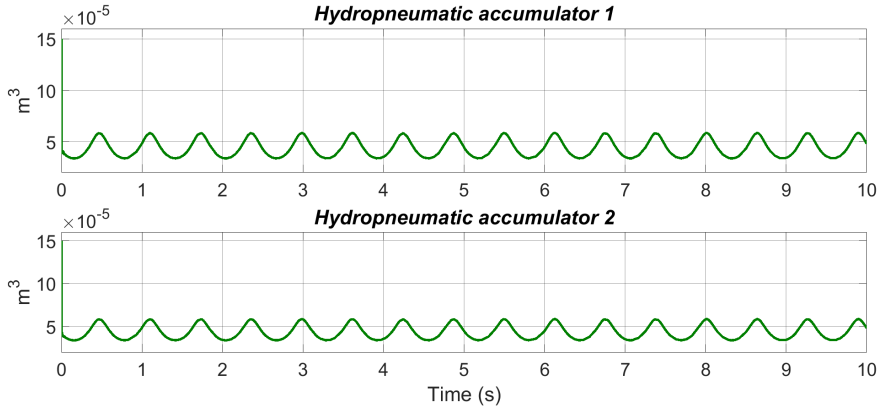

Figure 3.9: Volumes of gas contained in the HPAs

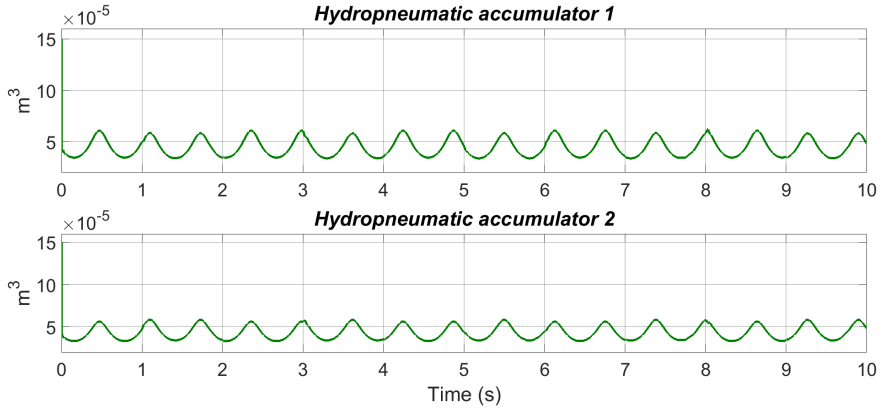

Figure 3.10: Volumes of gas contained in the HPAs with load force applied

The volumes are rapidly decreased since the desired stiffness of the system is higher than the one provided by the original pressures of the gases, enabling to state that the volumes are constantly adjusted to follow the stiffness.

3.3 Prototyping and possible applications

Two BMVSA has been prototyped in different scales: meso and micro, see Fig. 3.11. The meso-scale design is currently testing phase. Figure 3.12 shows a schematic of the implemented hydraulic circuit. Its main components are the hydraulic cylinder (*Cyl1*), a pair of HPAs (*AC1-2*), a hydraulic pump (*HyS*), two pressure gauges (*PG1-2*), four electro-proportional flow control valves (*EPF1-4*) and two

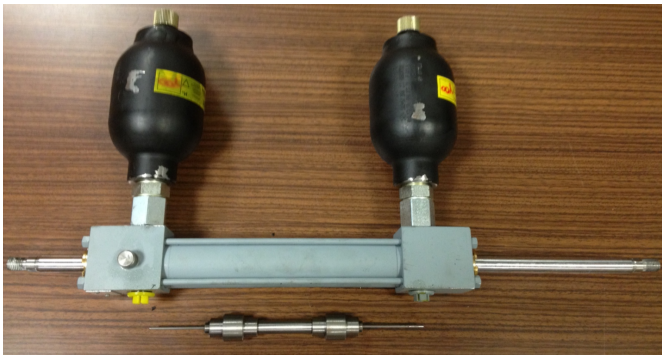

Figure 3.11: BMVSA prototypes. The actuator on the top is a meso-scale design while the one below one is a micro-scale.

proportional pressure control valves (*PC1-2*). The purpose of having two pressure control valves is to isolate the hydraulic input for each chamber of the cylinder.

The previously described model-based controller provides a solution for q_1 and q_2; to obtain the desired flows, a set of four *EPF* is used, two per chamber. The position of the piston is measured via encoder and the stiffness is calculated in real-time using the pressure gauges. Some of the targeted applications are related to service cobots, providing the systems with the inherent safety that the VSA provides. In the case of service robots, the loading force is minimal (2-3 kg maximum), requiring a small hydraulic supply unit and low pressures contained in the accumulators. For the cobot, the loading force is related to the task to be performed, which requires higher pressure from the supply unit and inside the accumulators.

Utilization of this VSA in rehabilitation devices for upper limb has also been considered [58, 59]. A compliant machine would allow the patient to perform small controlled tasks with the arms, imitating pronation and supination motions.

3.4 Conclusion

A VSA with inherent compliance can be designed using biphasic media as control fluids. The stiffness of the actuator is related to the pressures in the accumulators. The position and stiffness can be controlled using a logical pressure relation inside both hydraulic cylinder chambers. The hydraulic nature of the system gives it

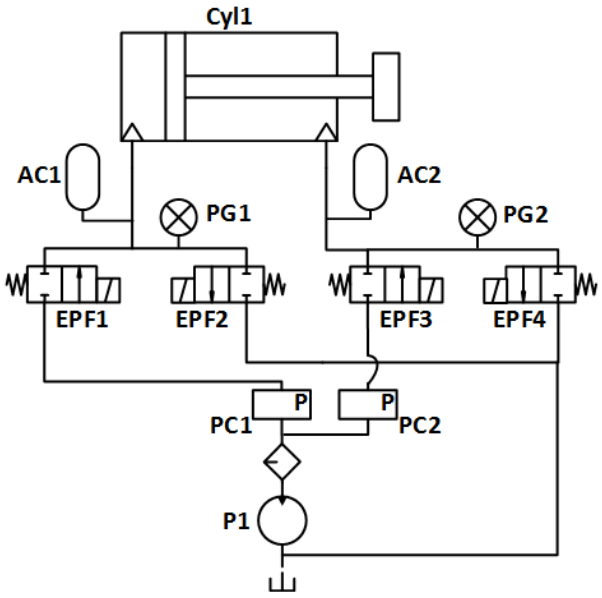

Figure 3.12: Hydraulic circuit diagram

the possibility to have a high output force, while the nonlinearity of the gas contained in the accumulators provides a bigger range of stiffness than the VSAs using traditional elastic components. The performed simulations of the system demonstrate that the model-based controller approach can accurately track desired position and stiffness, while an external force acts on it.

Chapter 4

Position and stiffness control of one DoF revolute joint using a BMVSA

This section presents a compliant revolute joint mechanism using a variable stiffness actuator. Equations relating to the dynamics of the mechanism are provided. Results from force loaded and unloaded simulations and experiments with a physical prototype are demonstrated.

4.1 Revolute joint

A revolute joint mechanism has been designed to visualize the effect of the stiffness variation of the actuator, as shown Fig. 4.1. This mechanism has one DoF and its geometric parameters are given in Table 4.1. Equations (4.1) and (4.2) relate linear displacement (xp) with angular displacement (θ).

$$cos(\theta_1) = \frac{C_o}{H_o} sin(\theta) + \frac{B_o}{H_o} cos(\theta) \tag{4.1}$$

$$x_p + L_o = \left(R_o^2 + H_o^2 - 2R_o H_o cos(\theta_1)\right)^{\frac{1}{2}} \tag{4.2}$$

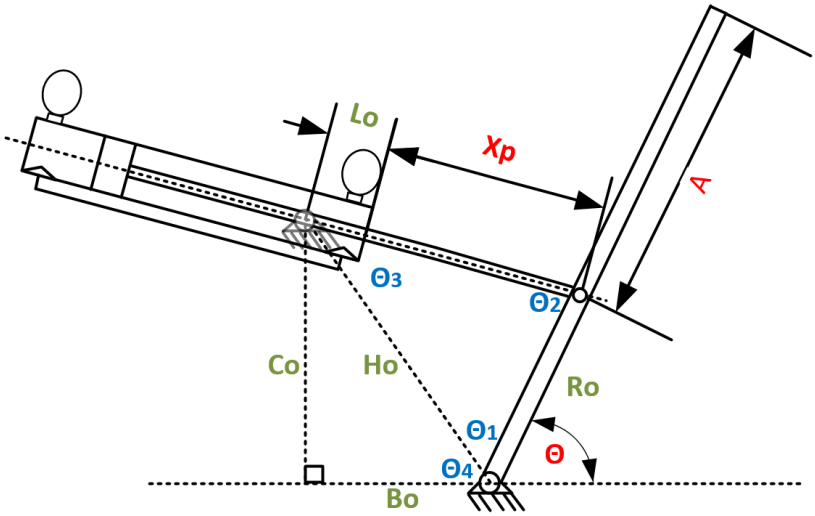

Figure 4.1: Diagram of revolute joint mechanism

4.1.1 Stiffness analysis

The output link works as a rotational actuator. Its torque, called τ_{joint}, is produced by F_p. Equations (4.3), (4.4), and (4.5) provide its definition.

$$\tau_{\text{joint}} = (SCR_o)\left(\frac{1}{v_1} - \frac{1}{v_2}\right) sin(\theta_2) \tag{4.3}$$

$$sin(\theta_2) = \frac{H_o}{x_p + L_o}\left(\frac{B_o}{H_o} sin(\theta) + \frac{C_o}{H_o} cos(\theta)\right) \tag{4.4}$$

Table 4.1: Geometric parameters

Parameter	Length (m)
L_o	0.07
C_o	0.1
B_o	0.105
H_o	0.145
R_o	0.12
A	0.245
$x_p$max	0.15
$x_p$min	0

$$\tau_{\text{joint}} = \tau_w + \tau_I + \tau_{F_{ext}} \tag{4.5}$$

τ_w is the torque generated by the weight of the equivalent mass, given by $m_{eq} = m_{\text{Load}} + m_{\text{Link}}$, at the center of mass ($R_{m_{eq}}$) on the output link, as shown in (4.6) and (4.7).

$$\tau_w = m_{eq} g R_{m_{eq}} sin\left(\frac{\pi}{2} - \theta\right) \tag{4.6}$$

$$R_{m_{eq}} = \left[m_{\text{Load}}\left(R_o + \frac{A_o}{2}\right) + m_{\text{Link}}\left(\frac{R_o}{2}\right)\right]\frac{1}{m_{eq}} \tag{4.7}$$

τ_I is the torque caused due to the inertia of the equivalent mass, as defined in (4.8). An external force has been considered to be applied at the end of the output link, producing $\tau_{F_{\text{ext}}}$, as shown in (4.9).

$$\tau_I = \frac{m_{eq} g (R_{m_{eq}})^2 \ddot{\theta}}{3} \tag{4.8}$$

$$\tau_{F_{\text{ext}}} = F_{\text{ext}}\left(R_o + A_o\right) \tag{4.9}$$

The instantaneous rotational stiffness $K(\theta)$ of the mechanism is the derivative of τ_{joint} with respect to the θ, as defined in (4.10).

$$K(\theta) = \frac{\partial \tau_{\text{joint}}}{\partial \theta} \tag{4.10}$$

The previous equations demonstrate that $K(\theta)$ is a function of the output force (F_p) and the angular displacement (θ), and it is affected by the weight of the equivalent mass.

4.2 Simulation

The following simulation was performed to study the stiffness and position of the model using the parameters given in Table 4.2. Two types of tests were performed: the first did not have an external force applied, while the second one had a force

Table 4.2: Simulation parameters for mechanism

Parameter	Value
m	$1\ Kg$
m_{Load}	$3.8\ Kg$
m_{Link}	$1\ Kg$
K_v	$0.5\ Ns/m$
K_E	$3x10^3\ N/m$
S	$3.776x10^{-4}\ m^2$
C	$300\ Pam^3$
γ	$-5x10^2$
λ	$-1.3x10^3$
$x_p(0)$	$0.075\ m$
$v_i(0)$	$1.5x10^{-4}\ m^3$

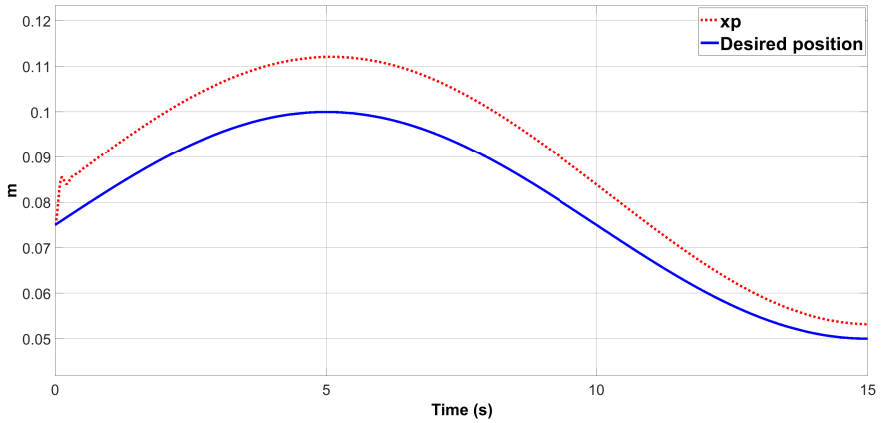

Figure 4.2: Position tracking in BMVSA without external force

signal with a square wave shape with 10 N amplitude and baseline on 0 N at 0.2 Hz. Both types of simulations were executed including the m_{Load} and m_{Link}. Position in the actuator is measured from left end of the cylinder to its right end.

The desired position is given as a sinusoidal signal with 0.23 radians amplitude and baseline on 1.23 radians at 0.05 Hz (to approximate a linear displacement in the cylinder with amplitude of 0.025 m and a baseline on 0.075 m), as shown in Figs. 4.2, 4.3, 4.4, and 4.5, while the desired stiffness is a sinusoidal signal with 20 Nm/radians amplitude and baseline on 80 Nm/radians at 0.1 Hz, as depicted in Fig. 4.6.

The results of the simulations prove that the model-based controller is able

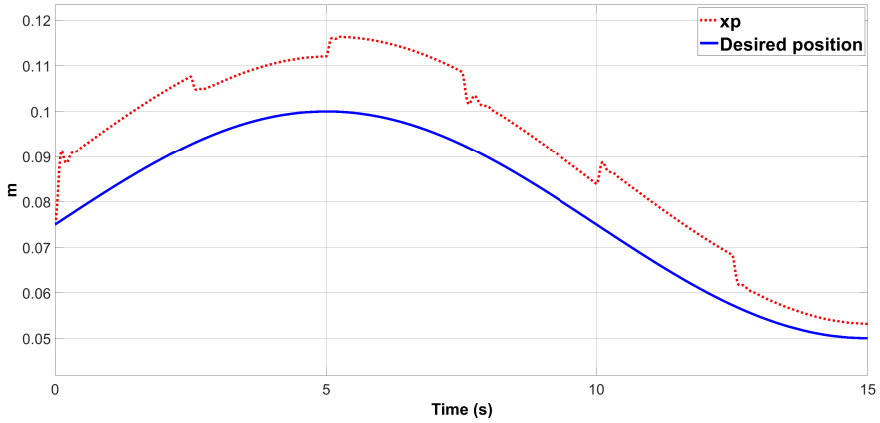

Figure 4.3: Position tracking in BMVSA with external force

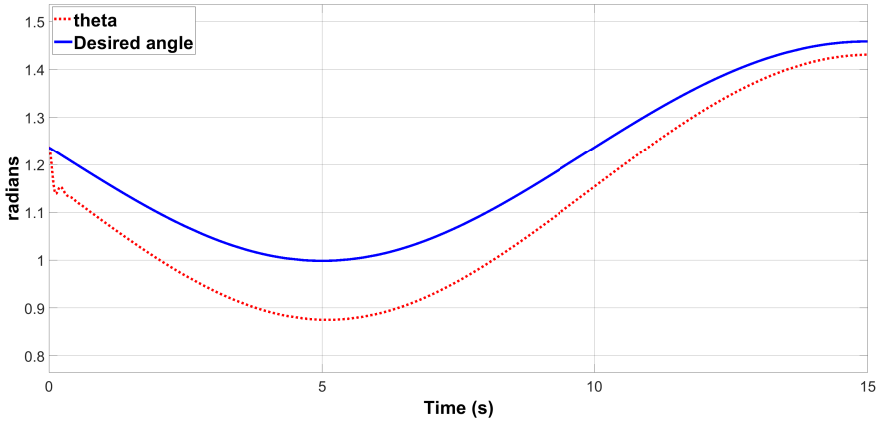

Figure 4.4: Angle tracking in mechanism without external force

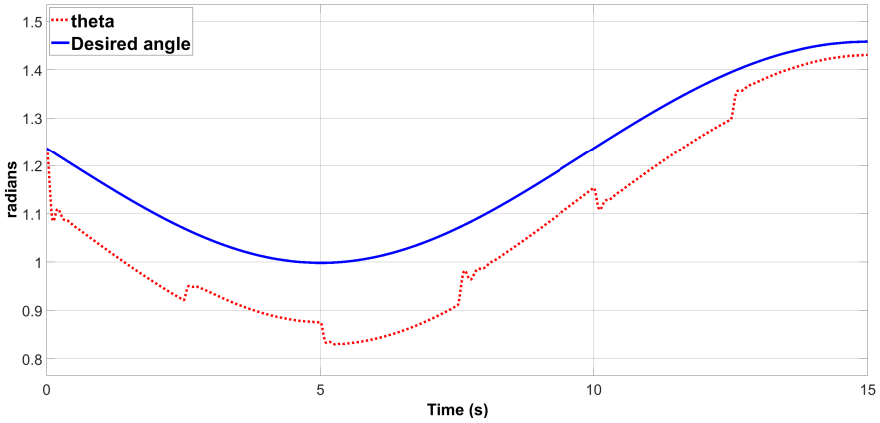

Figure 4.5: Angle tracking in mechanism with external force

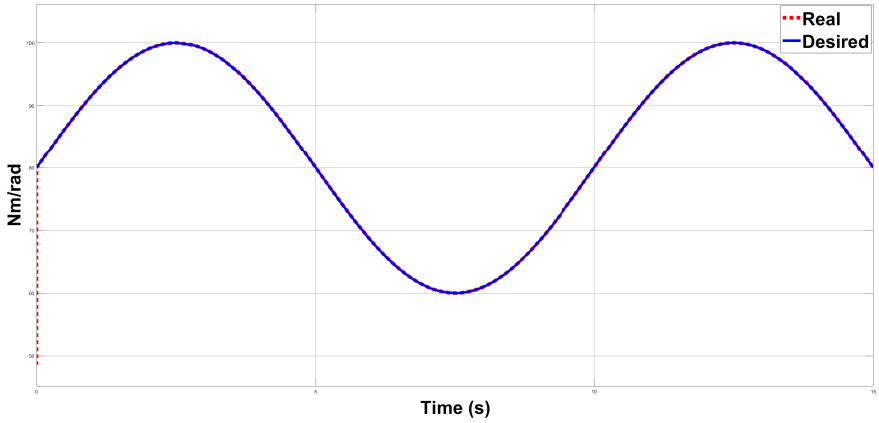

Figure 4.6: Stiffness tracking in mechanism without external force

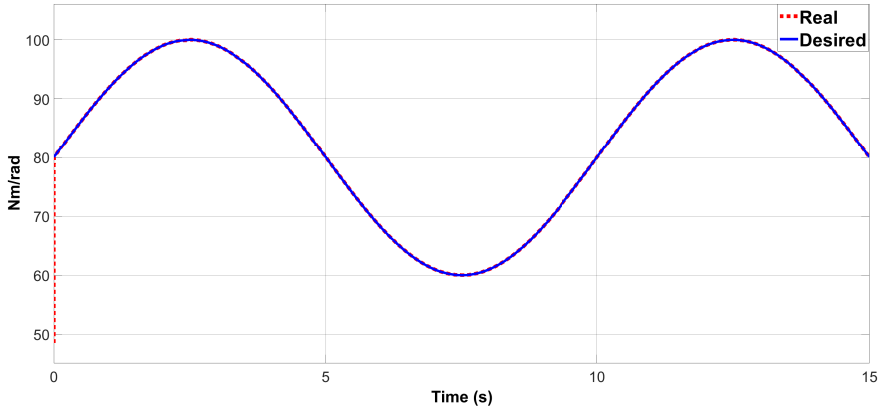

Figure 4.7: Stiffness tracking in mechanism with external force

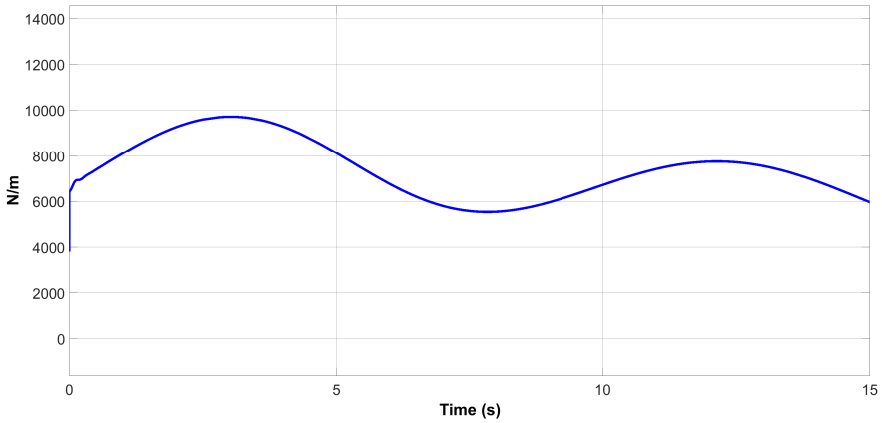

Figure 4.8: Stiffness tracking in BMVSA without external force

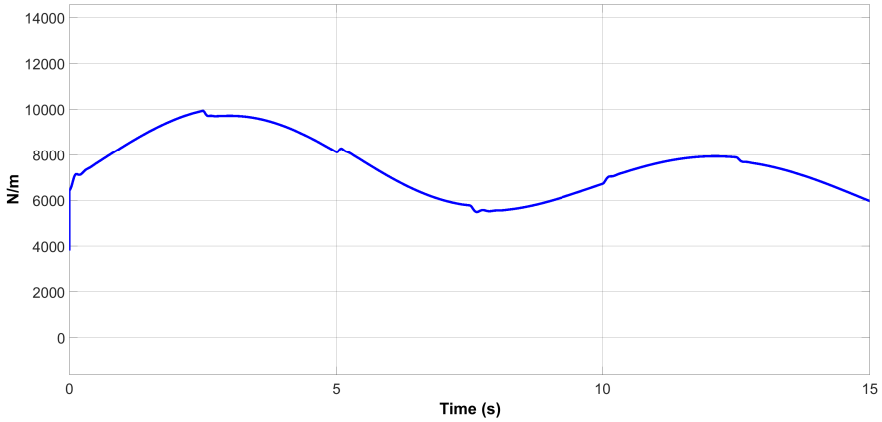

Figure 4.9: Stiffness tracking in BMVSA with external force

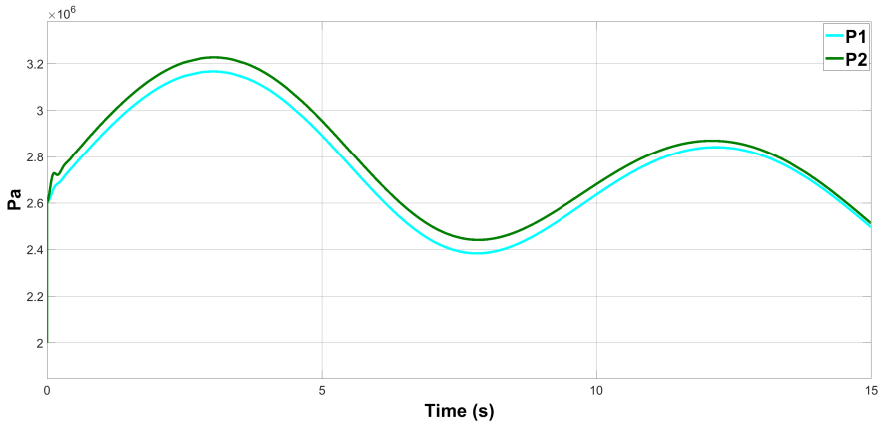

Figure 4.10: Pressures in BMVSA without external force

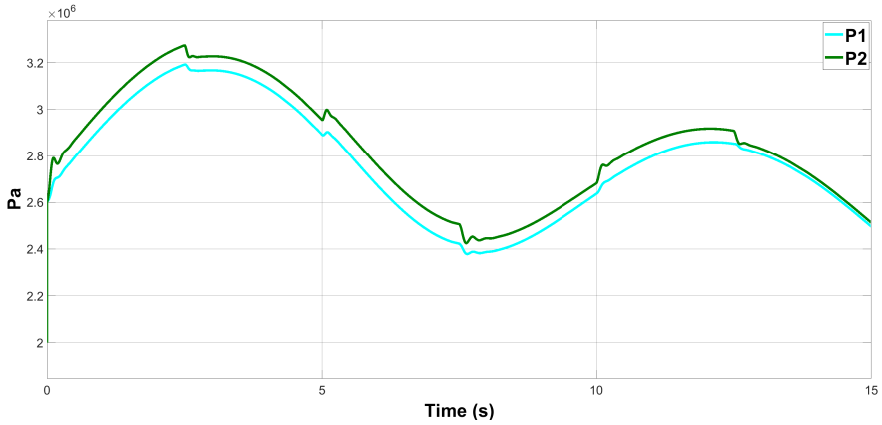

Figure 4.11: Pressures in BMVSA with external force

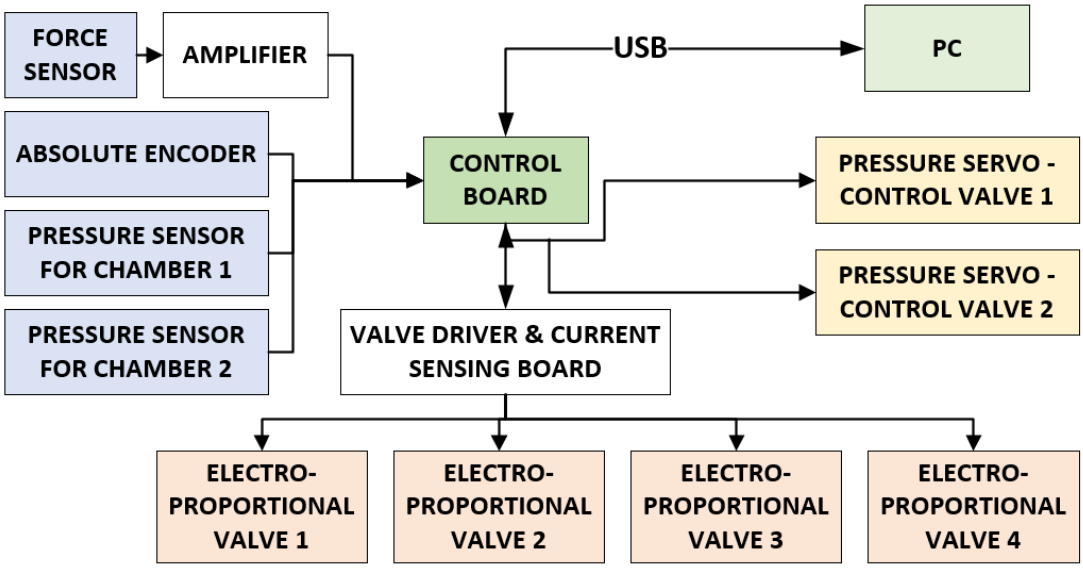

Figure 4.12: Experimental setup electronic control diagram

to properly track position and stiffness even if the desired signals to follow are nonlinear, as illustrated in Figs. 4.4 and 4.6. It is worth to note that the controller was tuned to prioritize stiffness tracking over position tracking as displayed in Fig. 4.3 and 4.5, where the desired position in never reached, while the desired mechanism stiffness is always obtained, see Fig. 4.7, 4.9 and 4.11. It can be stated that whenever a load force differs from zero a displacement in the actuator is generated, which is directly related to the value of K_E.

4.3 Prototype setup

The BMVSA and the mechanism have been prototyped and they are currently in testing phase, their composing elements are given in the bill of materials shown in Table 4.3 [60–64]. It is worthy to mention that most of the components are off-the-shelf, even the custom made control and valve driver boards can be replaced by industrial level control systems. The mechanism is made of steel and it keeps geometry and sizes mentioned in Table 4.1. The compression ratio (Co_R) is a physical characteristic of HPA that relates the maximum pressure that the accumulator can hold to its initial pressure before its rubber diaphragm wears

out considerably. Figure 3.12 shows a schematic of the implemented hydraulic circuit. Its main components were described in Chapter 3.3. The maximum flow, the maximum working pressure, the maximum difference of pressures between input and output and PWM frequency (10 liters/second, 350 bar, 15 bar, and 120 Hz, respectively for the selected valves) are *EPF*'s performance characteristics that limit the actuator to work within their physical limits. Fig. 4.16 shows the prototype in unloaded state.

The previously described model-based controller provides a solution for q_1 and q_2; to obtain the desired flows, a set of four *EPF* is used, two per chamber, see 4.13. The position of the piston is measured via encoder and the stiffness is calculated in real-time using the pressure gauges. The tuning parameters and initial conditions are given in Table 4.4. It is worth to mention that a pin shaped force gauge (*FG*) is used as the rotation pin that connects the cylinder and the arm. *FG* will be used for measuring the output force of the actuator in future experiments. A custom-designed control board powered by a multi-threaded ARM microprocessor is used to run the controller on real-time. This board contains drivers for valves running at 8 Hz for each of *EPF*. Figure 4.12 displays the electronic control diagram of the system, where, the main control component is the PC. The control board is used as an interface between the PC, sensors and valves. Figure 4.15 shows the valves driver and current sensing board, which its main function is provide coil's current measurements from each individual *EPF* valve in order to read its relative state to the control board, and control the flow of the same devices [65], its electronic diagram is given in Appendix B.

4.3.1 SWHARD control board

This board was by SWHARD s.r.l. and was intended for a prototyping use, having all the necessary components to develop a controller for the VSA plant [65, 66]. The structural block diagram of the board is presented in Appendix B. Its main characteristics are listed below.

- A STM32 microcontroller with an 32 bits ARM Cortex M4 running at 72 MHz with an external crystal.

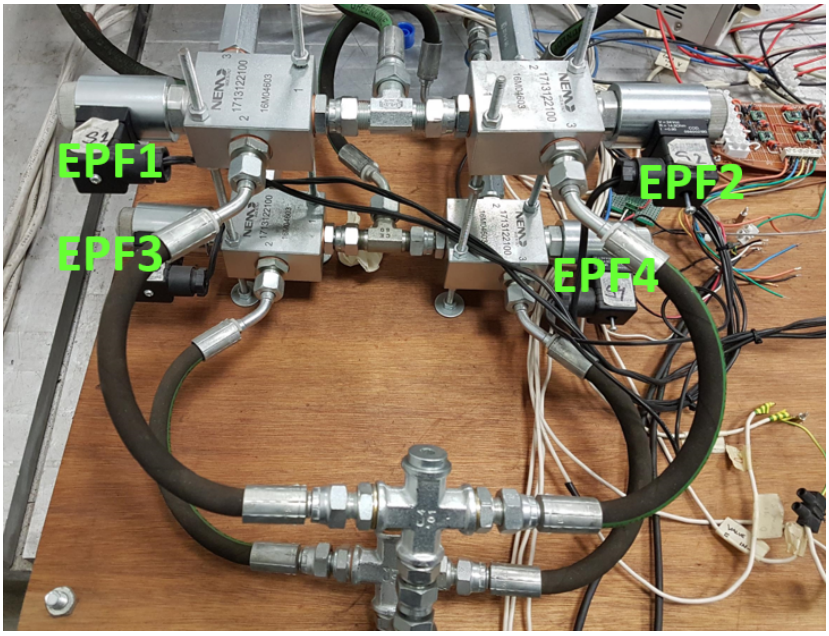

Figure 4.13: Electro-proportional valves array in the hydraulic circuit.

- On-board 3.3V and 12V linear regulators
- Digital Outputs (open-drain on power N-mosfets)
- Several external ADC with 8 channel , communicating to STM32 via SPI
- One 12V DAC, communicating with the STM32 via a SPI bus
- Interfaces for Avago encoders. The latter use the SSI protocol, a serial protocol compatible with SPI hardware
- A UART interface
- A USB port

4.4 Experiments with the prototype

Only loaded experiments were performed. A 3.8 kg metal bar is used to load the output link. Due to prototype's physical features, the desired position is given as

#	Component	Quantity	Model
1	Electro-proportional flow control valve	4	NEM 0353130101
2	Hydraulic pressure sensor	2	PU5401
3	Body for line mounting	4	NEM 1713122100
4	High pressure hydraulic hoses 1/4 in diam.	10	Generic hose. Different lengths are used
5	Pressure control valves	2	E-RI-TES
6	Hydraulic pump	1	Generic industrial model
7	Absolute encoder	1	AEAT-6010/6012 Magnetic Encoder
8	HPA	2	49-H-2014. Diaphragm type.
9	Double acting hydraulic cylinder	1	Custom made. It has fittings at both ends to connect HPA
10	Force gauge	1	Generic pin-shaped force sensor
11	Force gauge amplifier	1	Custom made, SWHARD design.
12	Power supply unit	1	Generic 24v-10A power supply

Table 4.3: Bill of materials

Figure 4.14: Hydraulic pump setup. A couple of pressure control valves are connected to the output of the pump to control the pressure that is provided to the system.

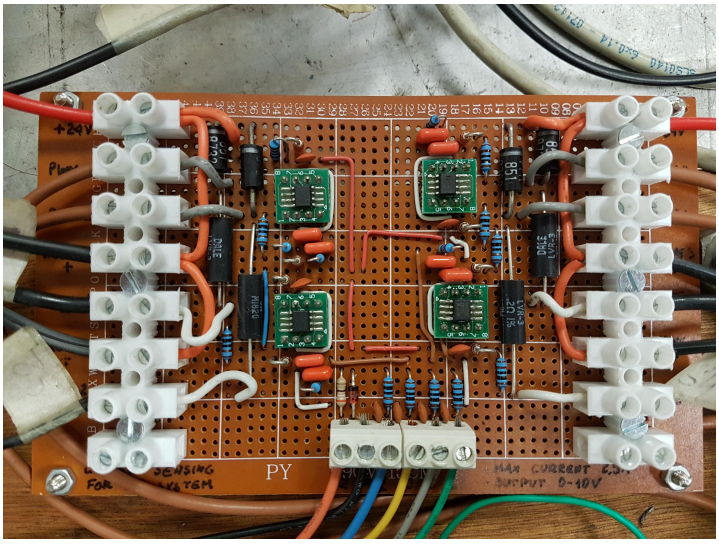

Figure 4.15: Valves driver board

a sinusoidal signal with 0.5 radians amplitude and baseline on 1.2 radians at 0.05 Hz, while the desired stiffness is a sinusoidal signal with 20 Nm/radians amplitude and baseline on 80 Nm/radians at 0.1 Hz.

The results of the experiments confirm that the model-based controller can track position and stiffness, as depicted in Figs. 4.17, 4.18, 4.19 and 4.20. Like in the simulations, the controller prioritized stiffness tracking over position tracking. Another presented phenomena that appear during the experiments are small jumps in the position, as shown 4.17 and 4.18, these are related to the static friction of the piston, the friction in mechanism joints, and the low frequency in which the *EPF*s work.

Table 4.4: Experiment parameters

Parameter	Value
K_v	$0.5\ Ns/m$
K_E	$2x10^4\ N/m$
γ	$-6.5x10^3$
λ	$-2.5x10^3$
$x_p(0)$	$0.075\ m$
Co_R	4

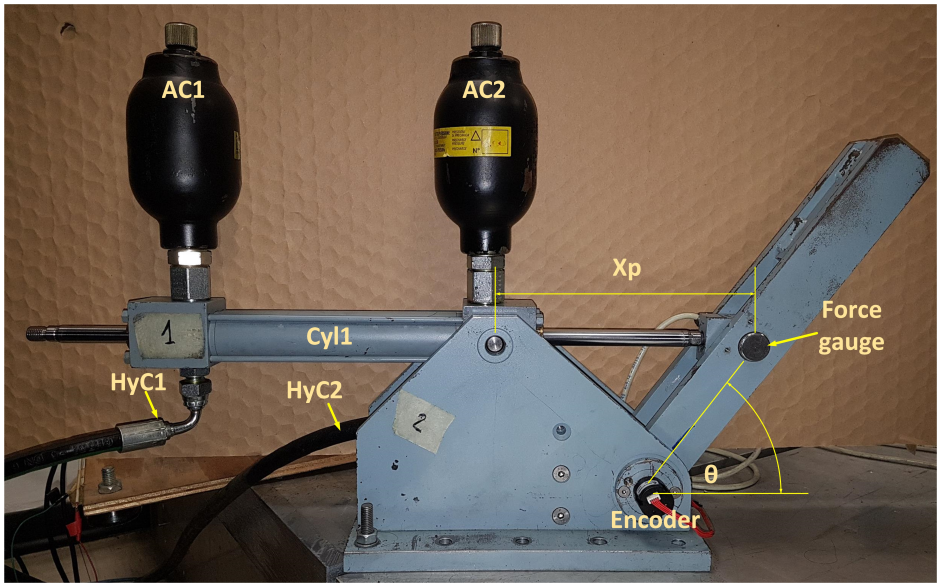

Figure 4.16: Prototype of mechanism

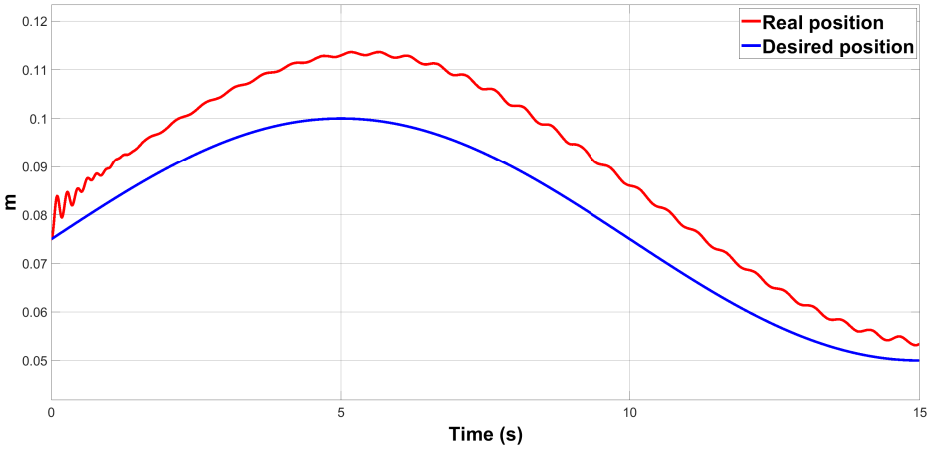

Figure 4.17: Position tracking during experiment

4.5 Conclusion

The results obtained from simulations demonstrate that the model-based controller approach can accurately track desired stiffness and approximate the desired position, while an external force acts on it. The measurements taken during the experiments corroborate the previously mentioned about the simulations, pointing out the influence of the output link's mass, friction and load's inertia.

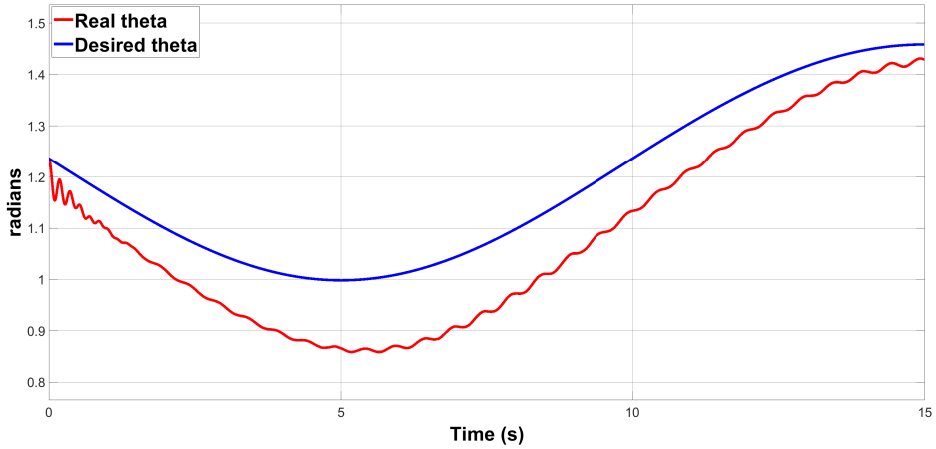

Figure 4.18: Angle tracking during experiment

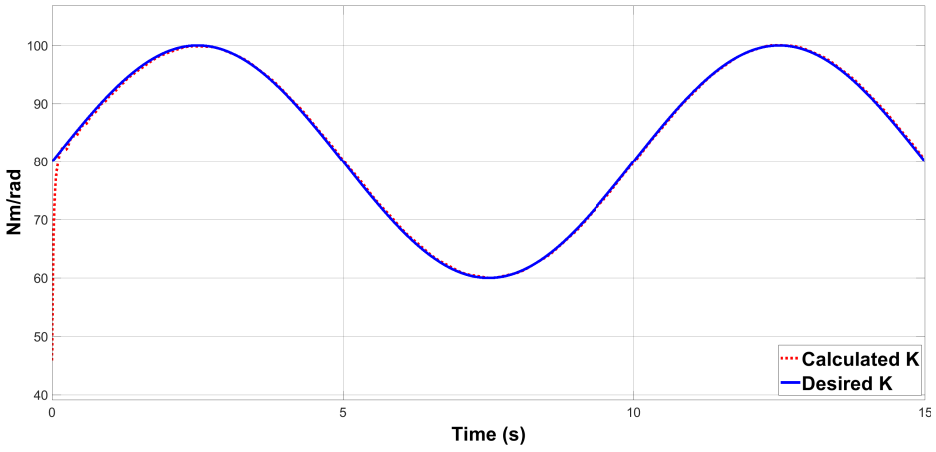

Figure 4.19: Estimated rotational stiffness tracking during experiment

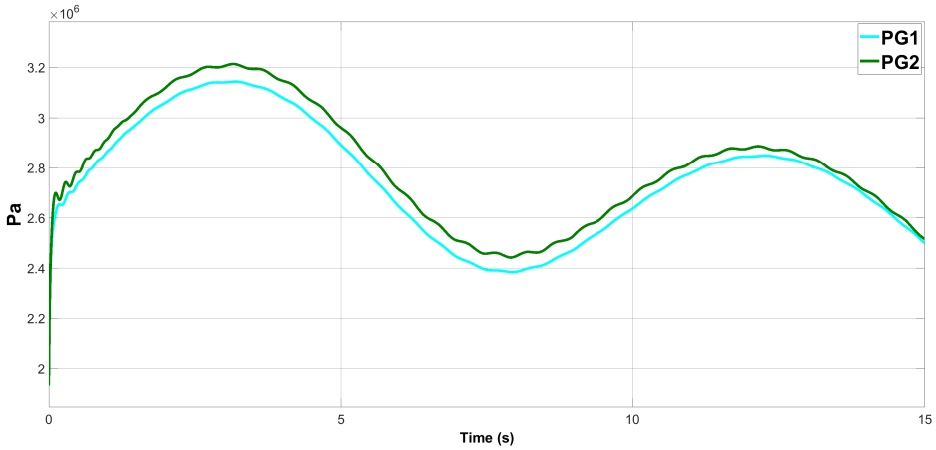

Figure 4.20: Measurements of pressure gauges

Chapter 5

Collision detection and reaction algorithms

VSAs are used to improve safety and performance in pHRI [67]. This protection is extended to unintended interactions due to hardware failure, limitations on perception and cognition [2]. Handling of collisions is one of the main objectives in pHRI because of the possibility of harming humans, causing damage to the environment or the robot itself.

5.1 Collision event process

Undesired collisions can be avoided by monitoring the workspace with external sensors to anticipate dangerous situations. Nevertheless, the use of exteroceptive sensors may not be sufficient to prevent collisions, since relative motions between robot and human could be fast and unpredictable [68]. When a direct and intentional human–robot interaction is desired, contacts are actually needed for task execution, requiring contact classification that distinguishes between intended and unintended contacts. For systematizing the contact handling problem, in [69] a unified framework entitled *the collision event pipeline* was proposed, which aims at embracing all relevant sequential phases collisions may undergo: (i)pre-collision or normal task operation,(ii) detection, (iii) isolation, (iv) identification, (v) classification, (vi) reaction, and (vii) post-collision. Some phases use monitoring

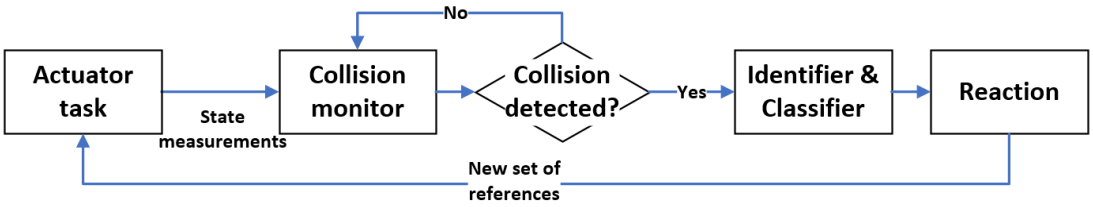

Figure 5.1: Collision event diagram

signals from the sensors and control devices in order to respond according to the context of the situation. Fig. 5.1 presents a reduced version of the pipe in a closed loop that is appropriate for an actuator level scenario. This scheme does not use an isolation phase due to the fact of being used for a single joint mechanism.

5.2 Collision detection

Collision detection is a phase, where an algorithm is fed with specific sensor's data and a binary output denoting the occurrence of a collision is given [69]. The occurrence of a collision must be detected as fast as possible. To avoid false positives and achieve high sensitivity an appropriate threshold on the monitoring signals must be tuned according to the current robot's task.

In [70, 71], an algorithm that only uses standard proprioceptive sensors was proposed for detection of collisions in robots; the detection also covered localization of the impact in the robot's structure. This algorithm consists in computing the expected torque and compare with the real one in order to get its residual. During free motion, all residuals are practically zero. The rising of one or more residuals above a fixed threshold corresponds to the occurrence of a collision. Residuals have the characteristic to rapidly return to zero as contact is lost. For faster collisions with stiffer environments, it is needed to analyze the transient phase following the first impact. This methodology is followed in [72], where a universal algorithm for sensorless collision detection of robot actuator faults is used to enhance the security of the robot.

Based on the work done in [67, 69], an actuator level abstraction of moment-based collision detector is implemented for BMVSA, as defined in (5.1). This

approach does not require the computation of accelerations and is able to detect collisions even when the velocity is zero. Another advantage of this method is that no extra sensors are required, the only needed quantities are x_p and P_i.

$$p(t) = m\dot{x}_p(t) \tag{5.1}$$

The monitoring signal r is the residual of the momentum and it is described in (5.2). K_I is a design parameter that allows r to closely follow the external disturbance (F).

$$r = K_I \left(p(t) - \int (F_p + r)dt - p(0) \right) \tag{5.2}$$

After r is computed, its absolute value is compared with a predefined threshold in order to indicate the existence of collisions.

5.3 Collision identification and classification

Relevant quantities about a collision are the directional information and the intensity of the collision force, either in terms of the acting Cartesian wrench at the contact or of the resulting external joint torque during the entire physical interaction event. This information characterizes the collision event and helps to interpret the collision nature in a context-dependent way, such as classifying the as accidental or intentional, light or severe, or even labeling its time course as permanent, transient, or repetitive.

If the collision involves human contact, standardized indices of injury severity can be used to classify the event. The most popular indices are Gadd Severity Index (GSI), the Head Injury Criterion (HIC), the ”3 ms” criterion, the Viscous Injury Response (VC), and the Thoracic Trauma Index (TTI) [32].

5.4 Collision reaction

The system must react purposefully in response to a collision event taking into account available contextual information. Because of the fast dynamics and high

uncertainty of the problem, the robot reaction should be embedded in the lowest control level. The most used reaction strategies are listed next.

- Stop movement. It is the simplest reaction. However, this may possibly lead to inconvenient situations, where the robot is constraining or blocking the crashed object.
- Slow down. Reduce the velocity of the system proportional to the level of the detected impact.
- Reflex control. This strategy drives back the robot for a longer movement, which would require the intervention of the kinetic energy dissipation phase.
- Impedance relaxation. The stiffness of the system is reduced proportional to the impact or directly up to a safe level.
- Task relaxation. The Cartesian task is preserved by only performing movements in the joint space. If the residual grows, the orientation is relaxed; if the residual grows to much, the full task is abandoned.
- Zero gravity. This strategy leaves the robot floating in space in response to the collision force, while motion is damped at the actuator side [73].

5.5 Collision detection simulation

The following simulation was performed to study the momentum-based collision detection algorithm (MBCDA) during a position and trajectory tracking task, these used values correspond to design parameters used to develop a prototype and are given in 5.1. A model-based controller, tuned for stiffness tracking priority, is used. The external forces are displayed in Fig. 5.2. It is worthwhile to mention that the disturbances differ in magnitude and duration. The desired position is given as a sinusoidal signal with 0.05 m amplitude and baseline on 0.075 m at 1 Hz, while the desired stiffness is a sinusoidal signal with 2.5x104 N/m amplitude and baseline on 5x104 N/m at 1 Hz.

The results of the simulations prove that MBC can properly track position and stiffness even when disturbances affect the system, as shown in Figs. 5.3, 5.4,

Table 5.1: Simulation parameters for collision events

Parameter	Value
m	1 Kg
K_v	0.5 Ns/m
K_E	2500 N/m
S	$3.776x10^{-4}$ m^2
C	300 Pam^3
γ	-70
λ	-100
$x_p(0)$	0 m
$x_{p_{max}}$	0.15 m
$x_{p_{min}}$	0 m
$v_i(0)$	$1.5x10^{-4}$ m^3
v_{imin}	$v_i(0)/4$ m^3
K_I	125 s^{-1}
$r_{threshold}$	30 N

and 5.5. The MBCDA effectively detected all the collision events whenever the absolute value of the residual overcomes to the predefined threshold, see Fig. 5.5. The threshold is shown as two symmetrical dotted parallel lines (pink and blue). Only the two disturbances that are between the threshold lines are not detected as collisions.

5.6 Collision experiments with prototype

The following collision event algorithm was implemented in the prototype developed in 4. The algorithm is composed of the following elements:

- MBCDA. It is tuned with only one threshold for the sake of simplicity.
- Stop motion reaction. The mechanism stops and tries to keep its position.
- Impedance relaxation reaction. The stiffness of the system is reduced to its minimum.

Classification of collisions was not realized because of the presence of only one threshold used in the detection. The parameters used for tuning the system

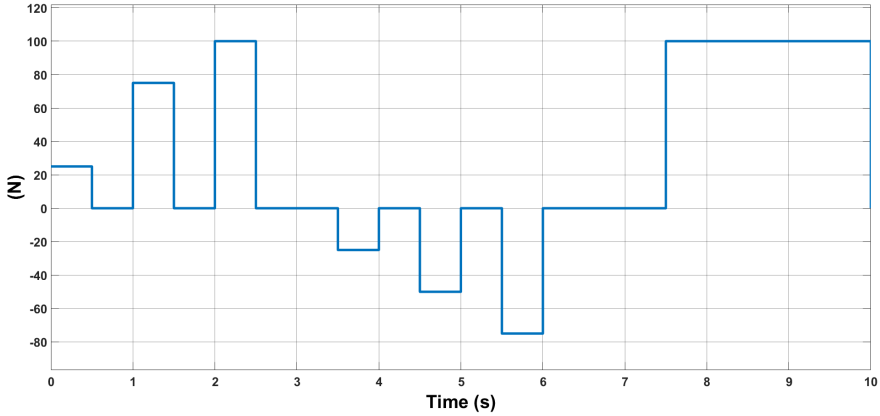

Figure 5.2: External force applied in the system

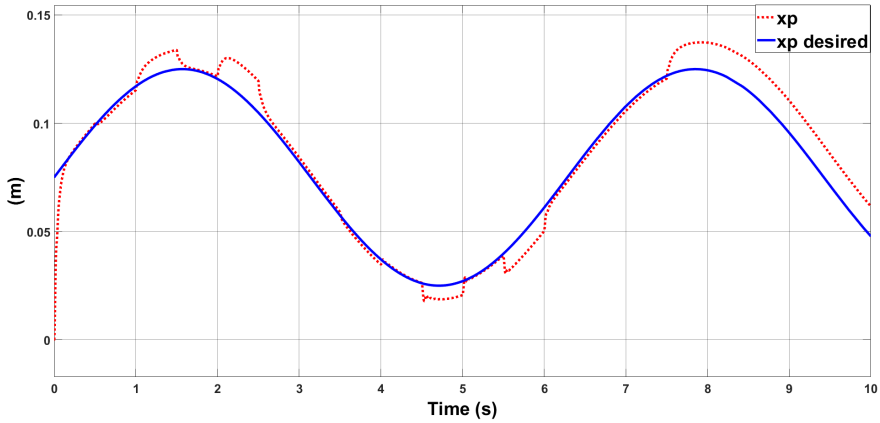

Figure 5.3: Position tracking during simulation

are given in Table 5.2. The reaction strategy is a combination of the previously defined reaction algorithms: stop the movement and keep the actual position as the new constant reference, while the stiffness of the device must drop to a safe value, in this case 4000 N/m. During the simulation, several forces of different magnitude impacted the arm of the mechanism, refer to Fig. 5.2. These forces were measured by the pin-shaped force gauge for only informative purpose. The sensors used to feedback the algorithm are the pressure gauges and the absolute encoder. The reference position is sinusoidal signal with 0.13 m amplitude and baseline on 0.075 m at 0.1 Hz, as shown in Fig. 5.7. The stiffness reference is a constant value of 20000 N/m.

The results of the experiments confirm that proposed collision event algorithm

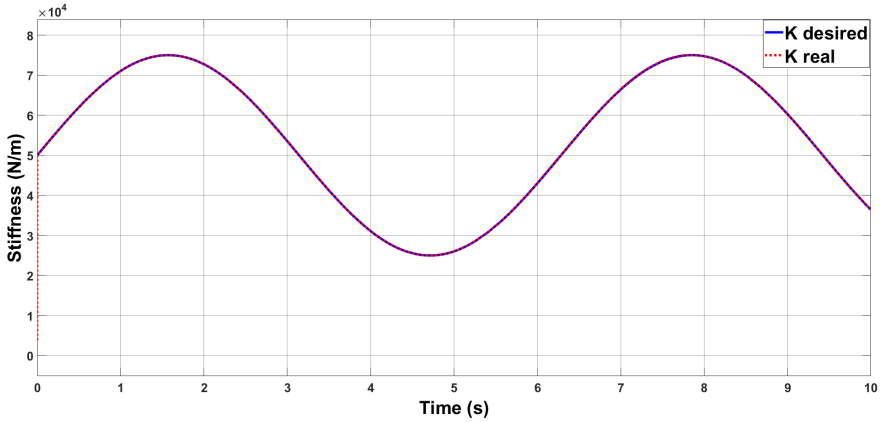

Figure 5.4: Experimental setup electronic control diagram

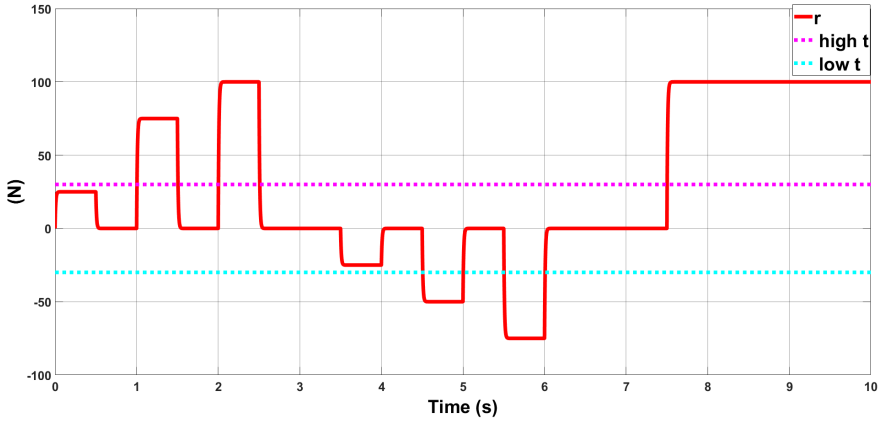

Figure 5.5: Residual graph with thresholds

Table 5.2: Parameters for collision experiments

Parameter	Value
K_E	20000 N/m
γ	-6800
λ	-2500
$x_p(0)$	0.14 m
K_I	1 s^{-1}
$r_{threshold}$	0.45 N

detects and reacts properly, as depicted in Figs. 5.7, 5.8, 5.9 and 5.10. Small disturbances in position during the experimentation are related to the static friction of the piston, the friction in mechanism joints, and the low frequency in

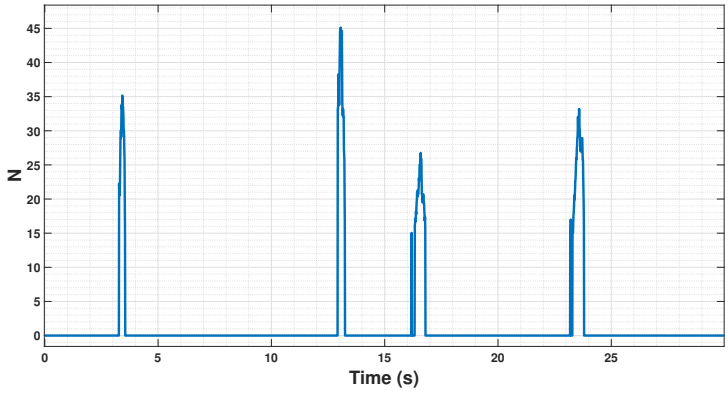

Figure 5.6: External force in collision experiment

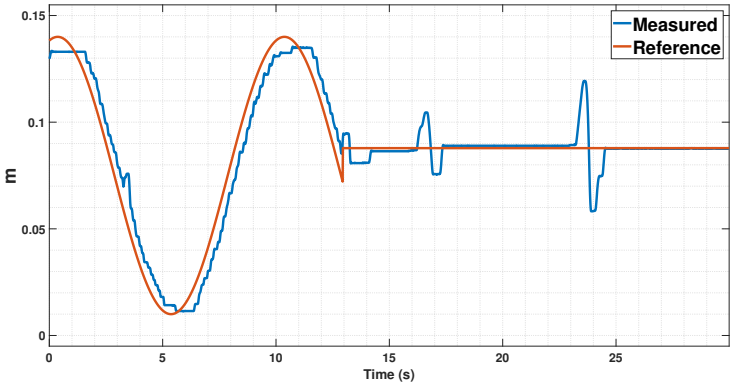

Figure 5.7: Position tracking in collision experiment

which the *EPF*s work.

5.7 Conclusions

MBCDA is a fast computing and efficient collision detector that makes use of the available sensors in the BMVSA. It is important to note the high impact of tuning of K_i and selecting $r_{threshold}$, which directly affects the quality of detection. Several thresholds can be established to classify the detected external force. The simulations and experiments demonstrate the feasibility of implementation of these type of algorithms at an actuator-level, leading to a more layered control structure of the complete system.

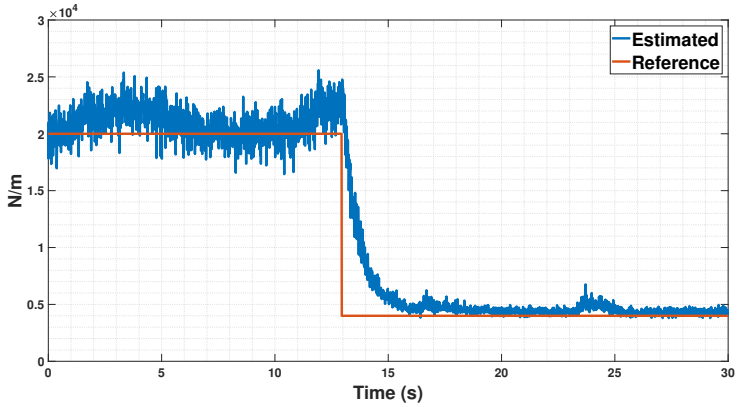

Figure 5.8: Stiffness tracking in collision experiment

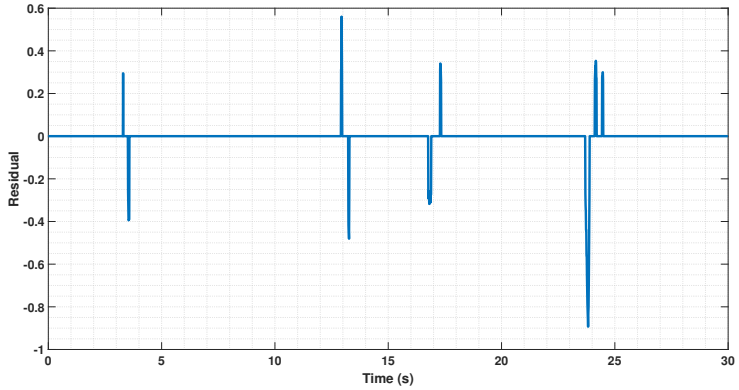

Figure 5.9: Residual in collision experiment

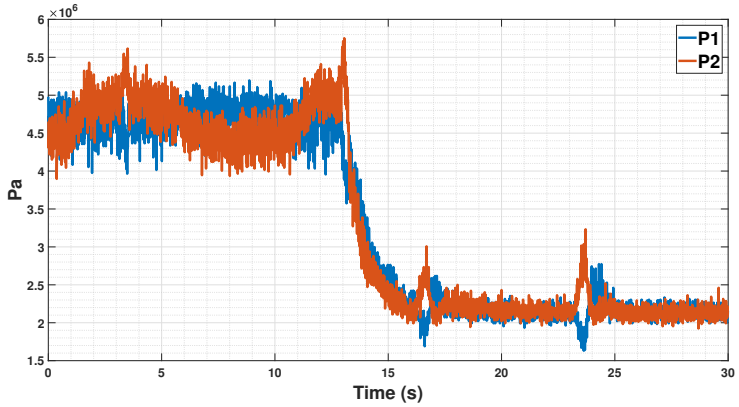

Figure 5.10: Pressure measurements in collision experiment

Chapter 6

Modeling of a cable-based revolute joint using BMVSA

In recent times, safe interactions between humans and robots are required for innumerable tasks and environments. This safety can be achieved using compliance design and control of mechanisms. Cable-driven mechanisms are used when applications need to have light structures, meaning that their actuators must be relocated to ground and forces are transferred along tensioned cables. This chapter presents a compliant cable-driven revolute joint using biphasic media variable stiffness actuators. Equations relating to the dynamics of the mechanism are provided with a joint stiffness and orientation controller. Results from simulations are discussed.

6.1 Introduction

Cable-driven manipulators are characterized by lightweight structure and adjustable stiffness. In [74], a compact variable stiffness device (VSD) is proposed to optimally control the stiffness of a two DoF cable-driven joint, see Fig. 6.1. It consists of one 4-bar rhombic mechanism and two springs. Link 1 and link 3, link 2 and link 4 are parallel with each other, respectively. The two springs connect to Link 1 and link 2, link 3 and link 4, respectively, which provide restoring forces and keep the device tight. VSD units with nonlinear stiffness characteristics have

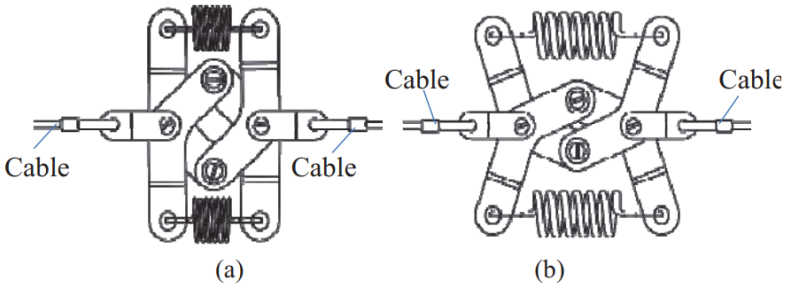

Figure 6.1: Deformations of VSD under different cable tensions. a) Low; b) High.

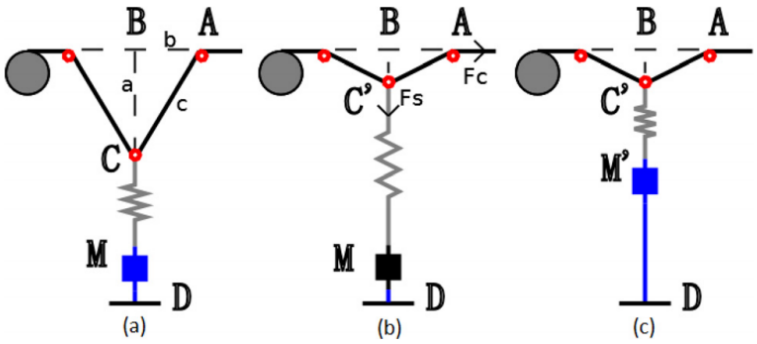

Figure 6.2: Variable stiffness module. (a) low stiffness configuration; (b) conventional passive module to achieve higher stiffness; and (c) active module to achieve higher stiffness with lower tension

been developed to adjust the compliance of cable-driven manipulators in [35, 75]. The total stiffness is given from cable stiffness and VSD by attaching in series a VSD along each cable of the manipulator. Robot's stiffness can thus be controlled by manipulating cable tensions. A cable-based active variable stiffness module is presented in [76]; its main characteristic is to have independent stiffness modulation with the desired tension due to controlled changes in structural parameters, as shown in 6.2. A comparison of modular-type antagonistic tendon-driven joints (TDJ) is detailed in [77] in order to design a new joint with higher stiffness and larger travel range than conventional TDJs.

6.2 Modeling of revolute joint

Thanks to the BMVSA's scalability, it is easy to use it instead of a hydraulic cylinder in order to gain variable stiffness. This allows the designer to try different mechanism architectures to develop more complex devices, like cable-driven joints. Based on the work done in [74, 76, 77], a simple antagonistic revolute joint was modeled, like the one displayed on Fig. 6.3. This tendon-driven mechanism is commonly actuated in three different modes:

1. One VSA pulls one cable and a passive device pulls the other one (spring, dead weight, etc.)
2. One stiff actuator is placed in series with a VSD for each cable
3. One VSA is used for each cable

The designed model uses the third mode to take advantage of the BMVSA stiffness range and maintain high-output force. The following assumptions were taken into account for developing the system: (i) the cables have uniform cross sections and are massless, (ii) there is not slippage between the cables and the pulley and (iii) BMVSAs can only pull. Pre-tensions (T_{pre_i}) are set in the cables to avoid slackening during motion, these forces are equal and do not influence joint's stiffness. The tensions in each cable are defined as the addition of the tension created by the VSA and the pre-tension of the cable, as shown in (6.1).

$$T_i = T_{VSA_i} + T_{pre_i} \tag{6.1}$$

This approach has the following kinematic constraints due to the fixed cable length.

$$\begin{aligned} \delta l_1 &= r\theta - x_{p1} \\ \delta l_2 &= -r\theta - x_{p2} \end{aligned} \tag{6.2}$$

where r is the radius of the pulley, θ is the rotation angle of the joint and l_i the length of the ith cable. The output torque of the joint is defined as the difference

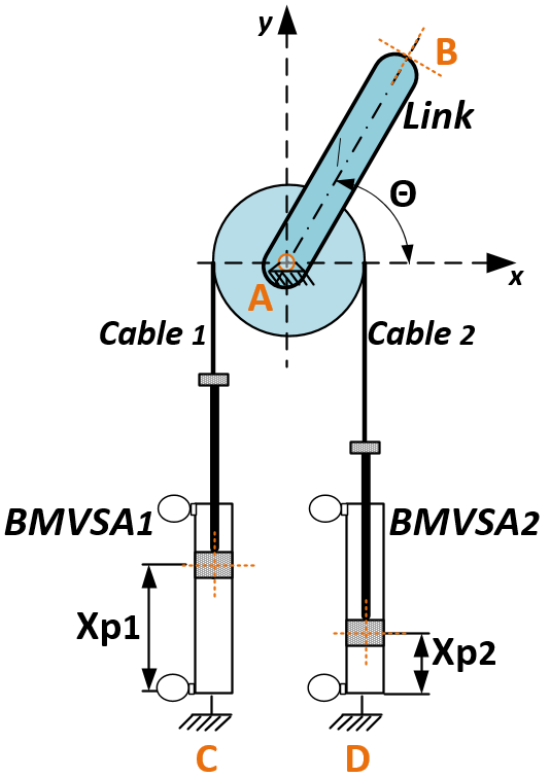

Figure 6.3: Diagram of cable-driven revolute joint. The location of the components is important for the design and force distribution in the system: A-center of pulley; B-end on link; C and D- VSA fixation places

of tensions in the cables as follows:

$$\tau = r(T_1 - T_2) \tag{6.3}$$

Finally, the stiffness of the joint is expressed in the equation below.

$$K_{joint} = r^2(K_1 + K_2) \tag{6.4}$$

6.3 Simulation of cable-driven joint

Only proprioceptive sensors of BMVSAs are taken into account for the simulation (encoders and pressure gauges); these sensors are enough to compute the joint

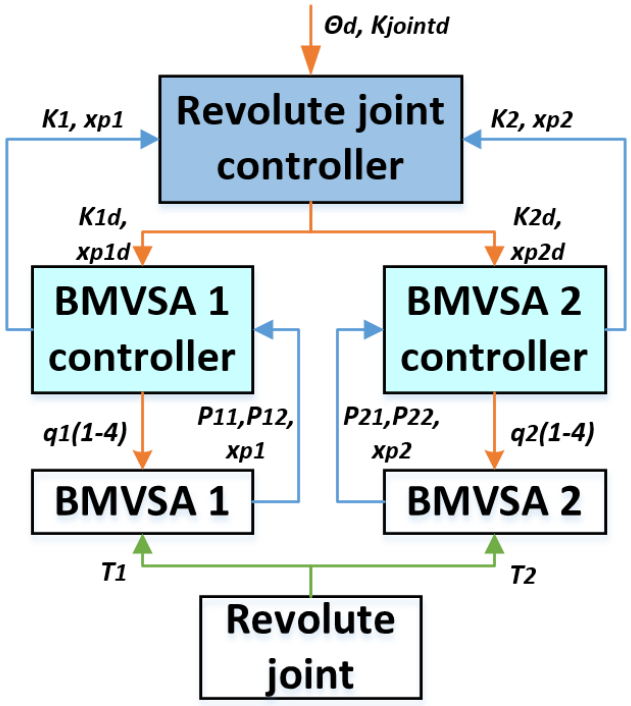

Figure 6.4: Control block diagram. Green arrows represent physical interactions, orange connections transmit references and blue arrows stand for measured and control signals

angle (θ), its stiffness (K_{joint}) and some external disturbance acting on the link (force or moment). The general control diagram is a leveled structure as shown in Fig. 6.4. The higher level contains the revolute joint controller (RJC), which receives the angle (θ_d) and joint stiffness (K_{joint_d}) from the user and feeds the BMVSA controllers with desired positions (x_{p_i}) and stiffness (K_i). The actuator level controllers, developed in section 3.1.3, provide the desired flows signals to the BMVSA and receives information from the pressure sensors and the encoders; these measurements also contain information of external disturbances coming from the revolute joint as variations in the cable tensions (T_i). To simplify the system, RJC calculates K_i equal for both actuators using eq. (6.4), and x_{p_i} with eq. (6.2). For tension's distribution during the application of an external disturbance, it is done by checking the sign of the generated moment and pulling from the corresponding cable to compensate.

The following simulation was performed to study the stiffness and position of

the joint using two equal BMVSAs with parameters given in Table 6.1, where $v_i(0)$ and v_{imin} are physical characteristics of real HPAs used in previous embodiments of the VSA. Figure 6.5 displays the reachable stiffness range of a single BMVSA, while Fig. 6.6 shows the conversion of the actuator stiffness into the cable-driven joint. It is noteworthy how the use of two BMVSA in the mechanism significantly increases the stiffness range.

The tests had an external disturbance represented by a moment with a square wave shape with 0.5 Nm amplitude and baseline on 0 Nm at 0.1 Hz, as shown in Fig. 6.7. Position in the actuators is measured from left end of the cylinder to its right end. The angle is given as a sinusoidal signal with $\pi/4$ radians amplitude and baseline on $\pi/2$ radians at 0.1 Hz, as displayed in Fig. 6.8, while the desired stiffness is a sinusoidal signal with 25 Nm/radians amplitude and baseline on 50 Nm/radians at 0.1 Hz, as depicted in Fig. 6.9.

The outcome of the simulations proves that RJC provided correct references to actuator controllers (Figs. 6.11 and 6.12) allowing the system to track position and stiffness even if the desired signals to follow are nonlinear. Figure 6.10 displays

Table 6.1: Simulation parameters for cable-driven joint

Parameter	**Value**
r	$0.0477\ m$
l_i	$0.175\ m$
l_{link}	$0.15\ m$
T_{pre_i}	$1\ N$
m	$1\ Kg$
K_v	$0.5\ Ns/m$
K_E	$2500\ N/m$
S	$3.776x10^{-4}\ m^2$
C	$300\ Pam^3$
γ	-70
λ	-100
$x_p(0)$	$0.075\ m$
$x_{p_{max}}$	$0.15\ m$
$x_{p_{min}}$	$0\ m$
$v_i(0)$	$1.5x10^{-4}\ m^3$
v_{imin}	$v_i(0)/4\ m^3$

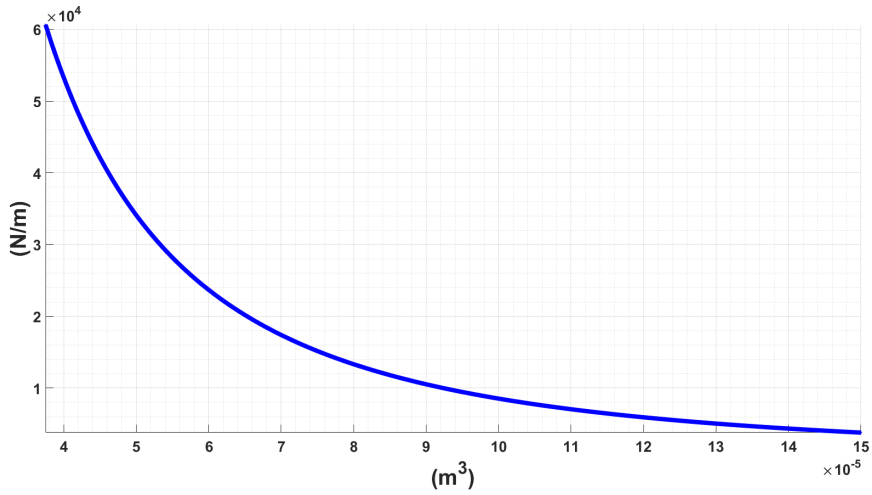

Figure 6.5: BMVSA stiffness range with respect to compressed volume of gas

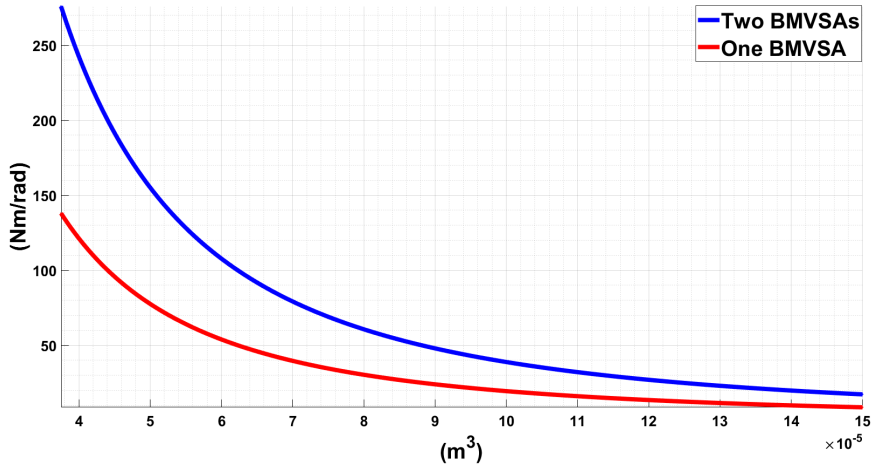

Figure 6.6: Cable-driven joint stiffness range using one or two BMVSA with respect to compressed volume of gas

the position of point B in X-Y plane; the importance of this point is due to its potential use as origin for a subsequent joint in a serial chain. Figures 6.7 and 6.13 reflect how the system is able to compensate an external disturbance by logically changing the tensions in the cables. It is worth to note that the controller prioritized stiffness tracking over position tracking, rendering the system unable to reach the position reference in the presence of disturbances, while the desired mechanism stiffness is always obtained, see Figs. 6.8, 6.11, 6.9 and 6.12.

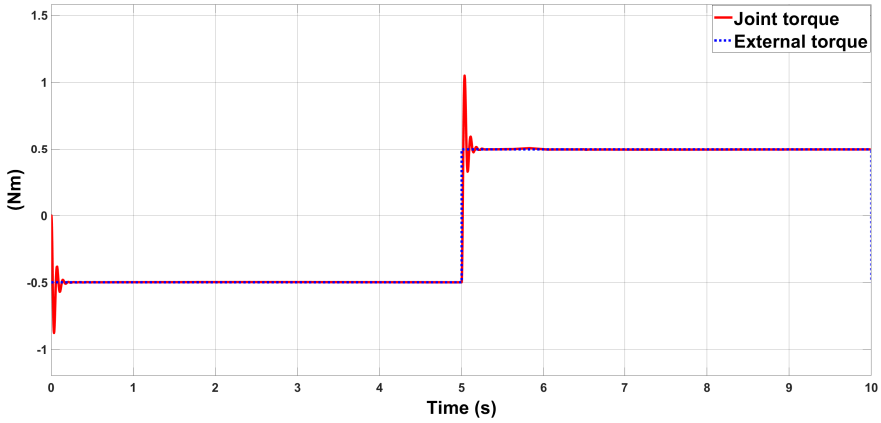

Figure 6.7: Joint torque. The joint torque is able to compensate the external torque with a minimum settling time

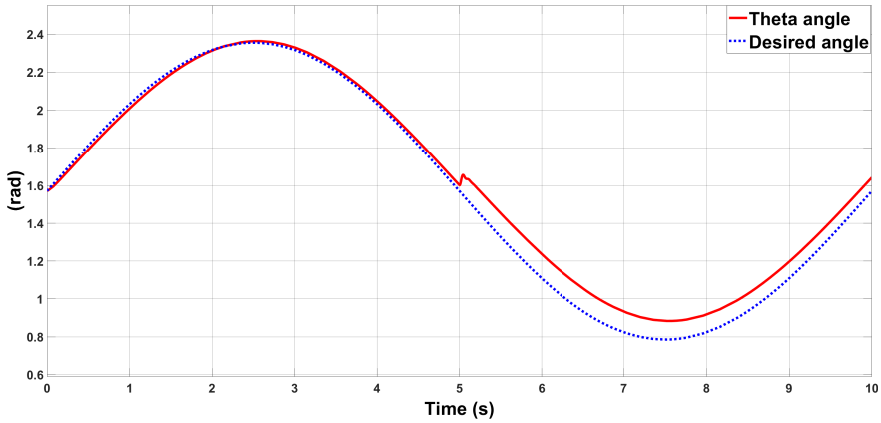

Figure 6.8: Joint angle. The desired angle is properly tracked but not reached due to the low stiffness of the system

6.4 Conclusions

Joint stiffness depends on the computed references for the BMVSAs. The cable-based revolute mechanism was modeled to take full advantage of the BMVSA characteristics to create a light weight and high output power joint. The results obtained from simulations demonstrate that the proposed controller approach can accurately track desired stiffness and approximate the desired position, even when an external force acts on it. Further work needs to be developed regarding the influence of the output link's mass, friction and load's inertia. A more accurate model including stiffness of the cable's material and the masses of the cables, pulley

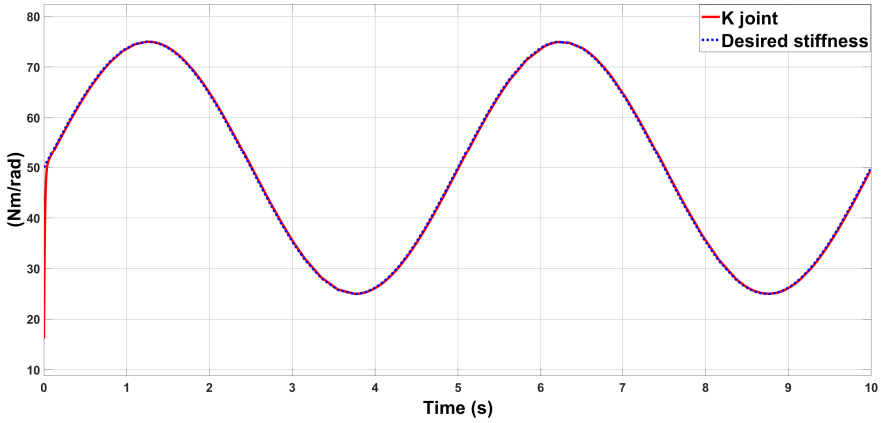

Figure 6.9: Joint stiffness tracking

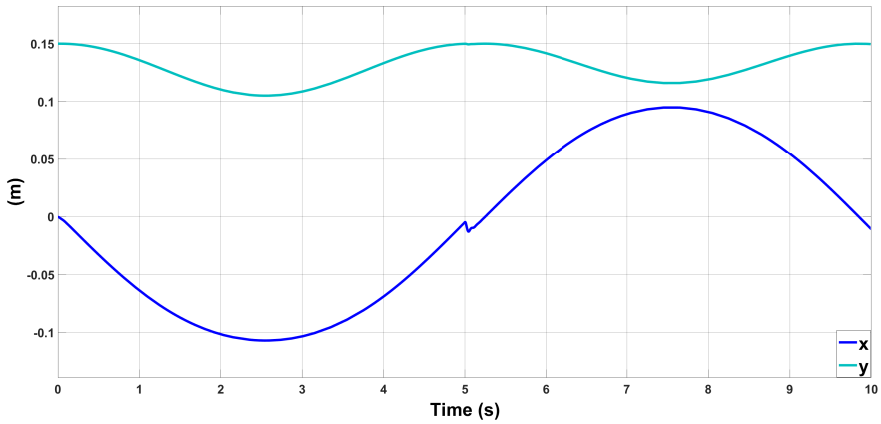

Figure 6.10: Position of point B

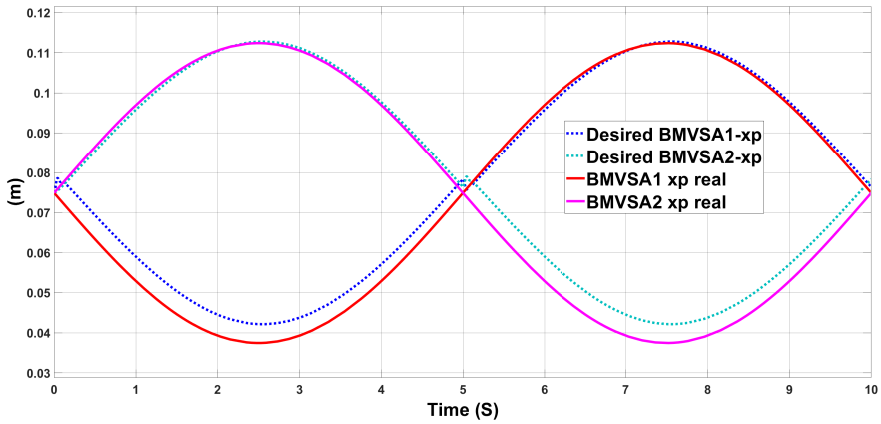

Figure 6.11: BMVSAs position tracking

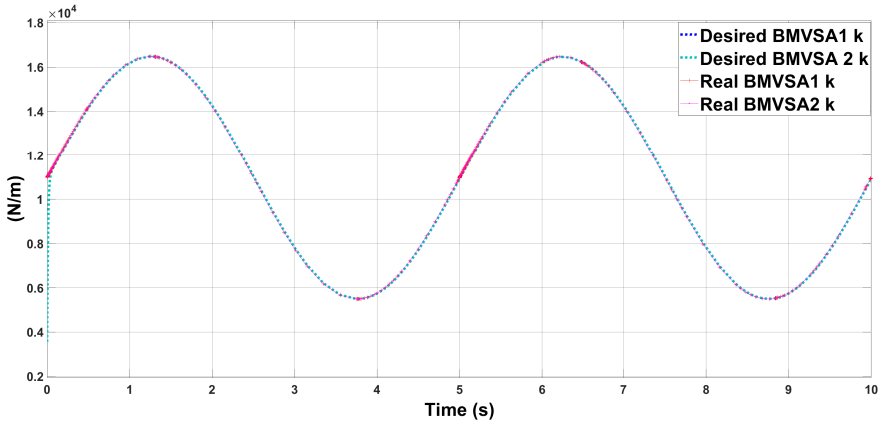

Figure 6.12: BMVSAs stiffness tracking

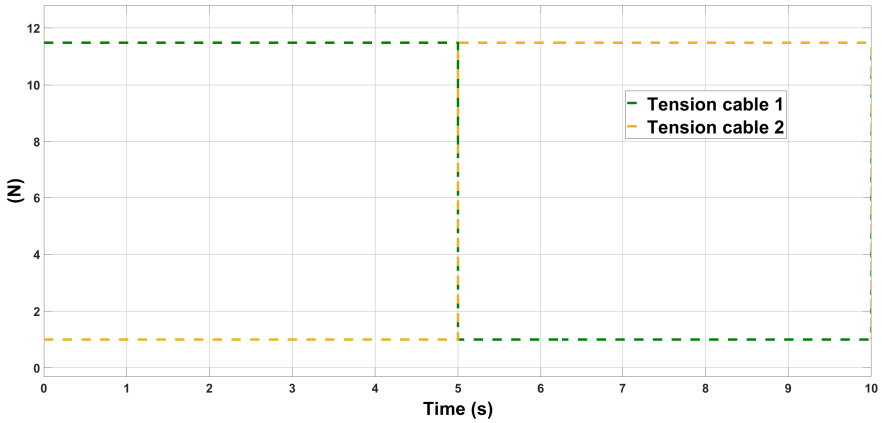

Figure 6.13: Tensions in cables. The tensions are never zero due to pre-tensioning

and link is being developed. This new approximation is expected to provide better understanding of the existing forces and help with the selection of components for prototype manufacturing.

Chapter 7

General conclusions

A VSA with inherent compliance can be designed using biphasic media as control fluids, where its stiffness is related to the pressures in the accumulators. The position and stiffness can be controlled by changing the pressure in both HPAs. The hydraulic nature of the system gives it the possibility to have a high output force, while the nonlinearity of the gas contained in the accumulators provides a bigger range of stiffness than the VSAs using traditional elastic components. Simulations of the system demonstrate that the model-based controller accurately tracks desired position and stiffness, while an external force acts on it. Results from the performed experiments with the device also proved that this controlling approach works fine and that mechanical adjustments must be done in the prototype to improve its behavior.

The collision event pipeline implementation demonstrates how the use of BMVSA can be extended in regards of safety and pHRI. The application of the BMVSA into a cable-driven mechanism demonstrates how the stiffness of the system can be manipulated just by replacing the stiff actuators.

Ongoing work is being done in the collision event pipeline project. A properly functioning algorithm covering the complete pipeline with an array of different reaction methods is expected to be implemented in the next couple of months.

A master thesis project titled *Design, prototyping, control and experiments of a 3 dof humanoid serial arm with biphasic variable stiffness actuation* has been approved and it is expected to start by the end of February, 2019. The objective of this project is to fully develop a cobot for general use. This activity belongs to

the European Master on Advanced Robotics program.

7.1 Future Research

Future developments related to the the ADCs and current sensing circuits in the SWHARD control board are being addressed in the next iteration of this control unit. The proper implementation of the electro-valves drivers is needed in order to improve its working frequency. A modular version of the software must be done in order to ease the extension of the project.

Modeling and design of rehabilitation devices and prosthesis is a well known application for VSAs. The technology developed in this project is expected to be part of the design of this kind of devices in collaboration with the School of Engineering of Autonomous University of San Luis Potosi. An internship at UASLP's Robotics and Mechatronics Laboratories will be performed after the thesis defense with this objective.

Appendix A

Friction in hydraulic cylinders

This section is meant to give a further explanation about damping in hydraulic cylinders. The friction force (F) is usually defined as a function of relative velocity and pressure. It is the sum of Stribeck, Coulomb (F_C), and viscous components [78]. The Coulomb friction consists of the preload force (F_p), caused by the seal squeeze during assembly, and the force proportional to pressure. The sum of the Coulomb and Stribeck friction forces at zero velocity is often referred to as the breakaway friction force. The friction is approximated with the equations below.

$$\begin{aligned} F &= F_C \left(1 + (K_b - 1)\, exp\left(-c_v|v|\right)\right) sign(v) + f_v v \\ F_C &= F_p + f_c(P_1 + P_2) \end{aligned} \tag{A.1}$$

where f_c is the Coulomb friction coefficient, P_1 and P_2 are the pressure in the cylinder's chambers, K_b is the breakaway friction coefficient, c_v is the transition coefficient, v is the relative velocity in the contact, and f_v is the viscous friction coefficient. To avoid discontinuity at $v = 0$, a small region $|v| \leqslant v_t$ is introduced around zero velocity, where friction is assumed to be linearly proportional to velocity.

$$\begin{aligned} F &= K_v v \\ K &= \frac{F_C \left(1 + (K_b - 1)\, exp\left(-c_v v_t\right)\right) + f_v v_t}{v_t} \end{aligned} \tag{A.2}$$

where K_v is the coefficient of proportionality and v_t is the velocity threshold. The following sections provide a deeper look into the physical origins of the previously defined forces.

A.1 Boundary friction

Also called dry or solid body friction. It is a resistive force against sliding in the interface between two solid bodies which are pressed onto each other by the normal force, their main causes are surface roughness and adhesion. The direction of the normal force (F_N)is perpendicular to the intended sliding direction, while the friction force (F_μ) acts opposed to the sliding [48]. There will be no movement in the interface as long as the tractive force (F_T) does not exceed a certain limit, known as static friction force $F_{\mu S}$, which does not contribute to the damping since it is only active at times without relative motion. The maximum static friction depends on the normal force and the coefficient of static friction μ_S, as displayed in (A.3).

$$F_{\mu S} = F_N \mu_S \tag{A.3}$$

$F_{\mu S}$ determines the minimum level of excitation below which a suspension system reduce acceleration. Static friction is normally caused by the sealing elements of the system, which must confine hydraulic pressure, creating a normal force that presses the sealing edge onto the respective opposite surface. This resistive effect worsens after long time intervals without operation.

When the F_T exceeds the $F_{\mu S}$, both solid bodies start to slide on each other and the sliding friction force ($F_{\mu G}$) appears, defined in (A.4). $F_{\mu G}$ is determined by the coefficient of sliding friction μ_G which depends on the properties of the sliding surfaces.

$$F_{\mu G} = F_N \mu_G \tag{A.4}$$

Due to the coincidence and counteraction of motion and sliding friction force, kinetic energy is transformed into heat. The higher the amount of energy stored

in the suspension system, the larger the amplitude of the oscillation. Due to the increased displacement, the energy drawn out of the system by friction during each oscillation increases with the stored energy.

A method to compensate for the amount of boundary friction is the integration of another spring-damper element in series to the hydraulic damper. A method to avoid stiction is proposed in [52], and consist in rotating the piston relative to the cylinder in situations where there is no relative axial velocity, eliminating stiction within a small interval around zero velocity in which a pure viscous behavior is obtained.

A.2 Fluid friction

Also known as viscous or hydrodynamic friction. It is generated when a flow resistor is placed in the flow path and causes internal fluid friction, causing a pressure increase upstream of the resistor. This additional pressure is acting upon the active areas of the cylinder thus creating a retarding force [48].

The pressure loss depends on the amount of volume flow through the flow resistor. This is the reason why the fluid friction depends significantly on the speed of the suspension motion. This means that a fluid friction damper adapts even twice to the amount of energy stored in an oscillation: by the amplitude of the oscillation and therefore indirectly secondly (for the same oscillation frequency) also by the velocity of the oscillation. Damping is preferred which is not depending upon fluid temperature. Therefore, at first sight a flow resistor with a strong orifice character seems to be the best choice.

A certain inevitable basic fluid damping of system is caused by the hydraulic lines and fittings between both ends, that depends upon the sizing of these components. Some systems with long distances between suspension cylinder and accumulator show only partly the potential effect which could be achievable with shorter or larger diameter lines. This explains the necessity to ensure that suspension cylinder and accumulator are positioned close to each other. The lower the basic damping, the better the possibilities for influencing the damping characteristic of a system by targeted integration of additional damping elements.

Appendix B

Prototype components

The structure of the control board designed by SWHARD is given in B.2. This diagram shows the main connections and blocks that compose the system. Figure B.1 provides the schematic of the electronic circuit of the current sensing board. Both of these devices are extensively described in [65, 66], covering the following important like electronic circuit design, firmware and communication design, simulations and experimentation.

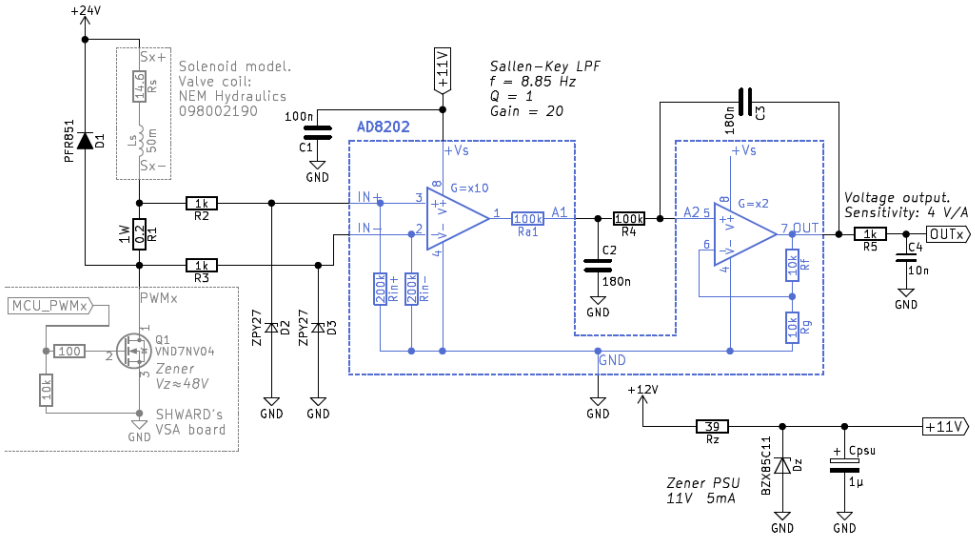

Figure B.1: Current sensing board schematic

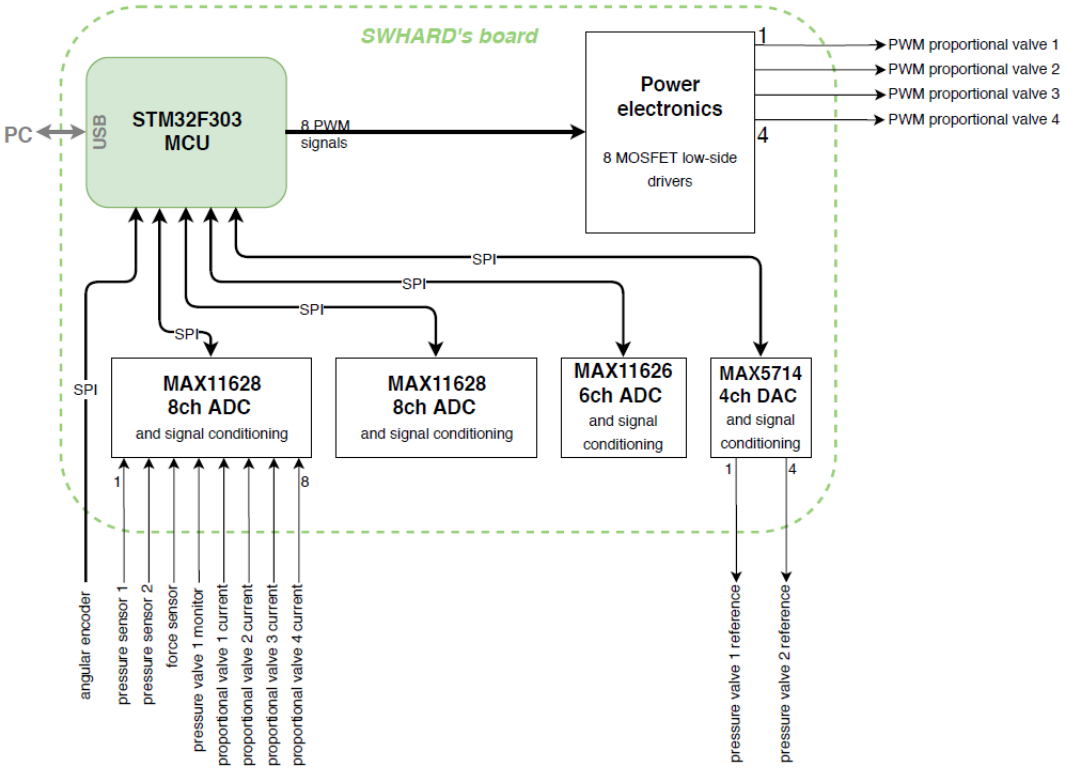

Figure B.2: SWHARD board diagram

Appendix C

Publications and related work

C.1 Modeling and Simulation of a Biphasic Media Variable Stiffness Actuator

- **Authors:** Jesus H. Lugo, Giorgio Cannata, Matteo Zoppi and Rezia Molfino.
- **Type of publication:** Article to be published in *International Journal of Mechanical Engineering and Robotics Research.*
- **Place and date:** Presented at *2018-7th International Conference on Mechatronics and Control Engineering (ICMCE 2018)*, Amsterdam, Netherlands, on November 28, 2018.
- **Abstract:**Nowadays, an increasing number of industrial processes are expected to have robots interacting safely with humans and the environment. Compliance control of robotic systems strongly addresses these scenarios. This article develops a variable stiffness actuator (VSA) whose position and stiffness can be controlled independently. The method for adapting the stiffness in the VSA includes a member configured to transmit motion that is connected to a fluidic circuit, into which a biphasic control fluid circulates. Actuator's stiffness is manipulated by varying pressure of control fluid into

distribution lines. The control fluid used is composed of gas and liquid, which are separated from each other and in proportions with predefined ratio. An approach for the mathematical model is introduced and a model-based control method is implemented to track the desired position and stiffness. Results from force loaded and unloaded simulations and possible applications of the system are discussed.

C.2 Position and stiffness control of one DoF revolute joint using a biphasic media variable stiffness actuator

- **Authors:** Jesus H. Lugo, Alessio Caligiuri, Matteo Zoppi, Giorgio Cannata and Rezia Molfino.
- **Type of publication:** Article to be published in *IEEE Computer Society Proceedings IRC 2019*.
- **Place and date:** Accepted for oral presentation at *Third IEEE International Conference on Robotic Computing (IRC 2019)*, Napoli, Italy, on November 25, 2019.
- **Abstract:**At this time, several industrial processes and service tasks need safe interactions between humans and robots. This safety can be achieved using compliance design and control of mechanisms. This paper presents a compliant revolute joint mechanism using a variable stiffness actuator. The method for adapting the stiffness in the actuator includes a member configured to transmit motion that is connected to a fluidic circuit, into which a biphasic control fluid circulates. Actuator's stiffness is controlled by changing pressure of control fluid into distribution lines. The used control fluid is biphasic, composed of separated gas and liquid fractions with predefined ratio. A mathematical model of the actuator is presented, a model-based

control method is implemented to track the desired position and stiffness, and equations relating to the dynamics of the mechanism are provided. Results from force loaded and unloaded simulations and experiments with a physical prototype are discussed.

C.3 Modeling of a cable-based revolute joint using biphasic media variable stiffness actuation

- **Authors:** Jesus H. Lugo, Vishal Ramadoss, Matteo Zoppi, Giorgio Cannata and Rezia Molfino.
- **Type of publication:** Article to be published in *IEEE Computer Society Proceedings IRC 2019.*
- **Place and date:** Accepted for oral presentation at *Third IEEE International Conference on Robotic Computing (IRC 2019)*, Napoli, Italy, on November 25, 2019.
- **Abstract:**Cable-driven mechanisms are used when applications need to have light structures, meaning that their actuators must be relocated to ground and forces are transferred along tensioned cables. This paper presents a compliant cable-driven revolute joint using biphasic media variable stiffness actuators. Actuator's stiffness is controlled by changing pressure of control fluid into distribution lines. The used control fluid is biphasic, composed of separated gas and liquid fractions with predefined ratio. The mathematical model of the actuator is presented along with its position and stiffness model-based control, then, equations relating to the dynamics of the mechanism are provided with a joint stiffness and orientation controller. Results from simulations are discussed.

C.4 Momentum-based collision detection algorithm for a biphasic media variable stiffness actuator

- **Authors:** Jesus H. Lugo, Matteo Zoppi and Rezia Molfino.
- **Type of publication:** Long abstract to be published in *Joint Workshop on New Technologies for Computer/Robot Assisted Surgery (CRAS).*
- **Place and date:** 2018-7th International Conference on Mechatronics and Control Engineering (ICMCE 2018), Genoa, Italy, on March 21, 2019.
- **Abstract:** Industrial collaborative robots and service assistant robots must be flexible and versatile to help humans in complex and demanding tasks. Variable stiffness actuators (VSA) are used to improve safety and performance in physical human-robot interaction (pHRI). This protection is extended to unintended interactions due to hardware failure, limitations on perception and cognition. Handling of collisions is one of the main objectives in pHRI because of the possibility of damaging humans, the environment or the robot itself. Collision detection is the second phase in the collision event pipeline, where an algorithm is fed with specific sensor's data and a binary output denoting the occurrence of a collision is given. To avoid false positives and achieve high sensitivity an appropriate threshold on the monitoring signals must be tuned according to the current robot's task. This abstract presents the application of a momentum-based collision detection algorithm (MBCDA) on a biphasic media variable stiffness actuator (BMVSA).

C.5 Design, implementation and experimental evaluation of a control system for a variable stiffness hydraulic actuator

- **Authors:** Alessio Caligiuri.
- **Type of publication:** Master thesis in Electronic Engineering.
- **Supervisors:** Giorgio Cannata, Matteo Zoppi, Egon Carusi and Jesus H. Lugo.
- **Place and date:** University of Genoa, Genoa, Italy, on December 21, 2018.
- **Abstract:**This thesis deals with a biphasic media VSA, whose regulation and implementation are discussed. Control models have been designed, simulated and implemented. In the aim of testing plant operation, an electronic control system has been integrated on a physical experimental setup, using a board provided by the company SWHARD. Furthermore, custom hardware and software have been developed, in order to provide all the tools necessary to conduct experiments and evaluate system performances

C.6 Design and analysis of biphasic media variable stiffness actuators

- **Authors:** Jesus H. Lugo, Giorgio Cannata, Matteo Zoppi and Rezia Molfino.
- **Status:** In processing.

C.7 Collision events handling using a biphasic media variable stiffness actuator

- **Authors:** Jesus H. Lugo, Giorgio Cannata, Matteo Zoppi and Rezia Molfino.
- **Status:** In processing.

C.8 Design, prototyping, control and experiments of a 3 dof humanoid serial arm with biphasic variable stiffness actuation

- **Authors:** Olena Hryshaienko.
- **Type of publication:** Master thesis in Advanced Robotics.
- **Status:** In processing.
- **Supervisors:** Giorgio Cannata, Matteo Zoppi and Jesus H. Lugo.
- **Place and date:** University of Genoa, Genoa, Italy, Summer of 2019.

References

[1] B. Vanderborght, A. Albu-Schäffer, A. Bicchi, E. Burdet, D. G. Caldwell, R. Carloni, M. Catalano, O. Eiberger, W. Friedl, G. Ganesh *et al.*, "Variable impedance actuators: A review," *Robotics and autonomous systems*, vol. 61, no. 12, pp. 1601–1614, 2013. 1, 6

[2] M. Zoppi, "Method for adapting stiffness in a variable stiffness actuator," Mar. 31 2015, uS Patent 8,991,169. 1, 6, 12, 49

[3] S. Sanan, "Soft inflatable robots for safe physical human interaction," Ph.D. dissertation, Carnegie Mellon University, 2013. 1

[4] R. Van Ham, T. G. Sugar, B. Vanderborght, K. W. Hollander, and D. Lefeber, "Compliant actuator designs," *IEEE Robotics & Automation Magazine*, vol. 16, no. 3, 2009. 1, 6, 7, 8, 9

[5] F. Platbrood and O. Görnemann, "Safe robotics – safety in collaborative robot systems," SICK AG White Paper, 06 2018. 2, 3, 5

[6] "Reducing robot risk: How to design a safe industrial environment," https://www.digikey.com/en/articles/techzone/2018/jan/reducing-robot-risk-how-to-design-a-safe-industrial-environment, accessed: 2019-01-22. 2

[7] J. D. Millar, "Request for assistance in preventing the injury of workers by robots," National Institute for Occupational Safety and Health, 12 1984. 2

[8] A. N. S. Institute, *ANSI/RIA R15. 06-1999: American National Standard for Industrial Robots and Robot Systems, Safety Requirements.* Robotic Industries Association, 1999. 2

[9] I. Iso, "Iso 10218-1: 2011: Robots and robotic devices–safety requirements for industrial robots–part 1: Robots," *Geneva, Switzerland: International Organization for Standardization*, 2011. 3

[10] I. ISO, "10218-2: 2011: Robots and robotic devices–safety requirements for industrial robots–part 2: Robot systems and integration," *Geneva, Switzerland: International Organization for Standardization*, 2011. 3

[11] A. De Santis, B. Siciliano, A. De Luca, and A. Bicchi, "An atlas of physical human–robot interaction," *Mechanism and Machine Theory*, vol. 43, no. 3, pp. 253–270, 2008. 3, 5

[12] V. Murashov, F. Hearl, and J. Howard, "Working safely with robot workers: Recommendations for the new workplace," *Journal of occupational and environmental hygiene*, vol. 13, no. 3, pp. D61–D71, 2016. 3

[13] A. Cherubini, R. Passama, A. Crosnier, A. Lasnier, and P. Fraisse, "Collaborative manufacturing with physical human–robot interaction," *Robotics and Computer-Integrated Manufacturing*, vol. 40, pp. 1–13, 2016. 3

[14] I. Maurtua, A. Ibarguren, J. Kildal, L. Susperregi, and B. Sierra, "Human–robot collaboration in industrial applications: Safety, interaction and trust," *International Journal of Advanced Robotic Systems*, vol. 14, no. 4, p. 1729881417716010, 2017. 3

[15] "Yumi® - irb 14000," https://new.abb.com/products/robotics/industrial-robots/yumi, accessed: 2019-01-22. 4

[16] G. Virk and S. Cameron, "Iso-iec standardization efforts in robotics," *INTERNATIONAL PROGRAM COMMITTEE*, p. 5, 2014. 3

[17] T. Jacobs and G. S. Virk, "Iso 13482-the new safety standard for personal care robots," in *ISR/Robotik 2014; 41st International Symposium on Robotics; Proceedings of.* VDE, 2014, pp. 1–6. 3

[18] "Care-o-bot 4," https://www.care-o-bot.de/en/care-o-bot-4.html, accessed: 2019-01-22. 4

[19] "Pepper robot-softbank robotics," https://en.wikipedia.org/wiki/Pepper˙(robot), accessed: 2019-01-22. 4

[20] A. Albu-Schaffer, A. Bicchi, G. Boccadamo, R. Chatila, A. De Luca, A. De Santis, G. Giralt, G. Hirzinger, V. Lippiello, R. Mattone *et al.*, "Physical human-robot interaction in anthropic domains: safety and dependability," in *Proceeding 4th IARP/IEEE-EURON Workshop on Technical Challenges for Dependable Robots in Human Environments*, 2005. 5

[21] B. Vanderborght, R. Van Ham, D. Lefeber, T. G. Sugar, and K. W. Hollander, "Comparison of mechanical design and energy consumption of adaptable, passive-compliant actuators," *The International Journal of Robotics Research*, vol. 28, no. 1, pp. 90–103, 2009. 6

[22] A. Bicchi, S. L. Rizzini, and G. Tonietti, "Compliant design for intrinsic safety: general issues and preliminary design," in *IROS*, 2001. 6

[23] S. Wolf, T. Bahls, M. Chalon, W. Friedl, M. Grebenstein, H. Höppner, M. Kühne, D. Lakatos, N. Mansfeld, M. C. Özparpucu *et al.*, "Soft robotics with variable stiffness actuators: tough robots for soft human robot interaction," in *Soft Robotics*. Springer, 2015, pp. 231–254. 6

[24] L. Le, M. Zoppi, M. Jilich, H. Bo, D. Zlatanov, and R. Molfino, "Application of a biphasic actuator in the design of the clopema robot gripper," *Journal of Mechanisms and Robotics*, vol. 7, no. 1, p. 011011, 2015. 6

[25] ——, "Application of a biphasic actuator in the design of a robot gripper for garment handling," in *ASME 2014 International Design Engineering Technical Conferences and Computers and Information in Engineering Conference*. American Society of Mechanical Engineers, 2014, pp. V05BT08A022–V05BT08A022. 6

[26] L. Le, M. Zoppi, M. Jilich, R. Camoriano, D. Zlatanov, and R. Molfino, "Development and analysis of a new specialized gripper mechanism for garment

handling," in *ASME 2013 International Design Engineering Technical Conferences and Computers and Information in Engineering Conference*. American Society of Mechanical Engineers, 2013, pp. V06BT07A013–V06BT07A013. 6

[27] B. Han, M. Zoppi, and R. Molfino, "Variable impedance actuation meso-micro physical models and rotation link using biphasic media," *Procedia Engineering*, vol. 64, pp. 1020–1029, 2013. 6

[28] R. R. Torrealba, S. B. Udelman, and E. D. Fonseca-Rojas, "Design of variable impedance actuator for knee joint of a portable human gait rehabilitation exoskeleton," *Mechanism and Machine Theory*, vol. 116, pp. 248–261, 2017. 6

[29] M. Cestari Soto, "Variable-stiffness joints with embedded force sensor for high-performance wearable gait exoskeletons," Ph.D. dissertation, 01 2017. 6

[30] E. Garcia, J. C. Arevalo, F. Sanchez, J. Sarria, and P. Gonzalez-de Santos, "Design and development of a biomimetic leg using hybrid actuators," in *Intelligent Robots and Systems (IROS), 2011 IEEE/RSJ International Conference on*. IEEE, 2011, pp. 1507–1512. 6

[31] B. Han, M. Zoppi, and R. Molfino, "Variable impedance actuation using biphasic media," *Mechanism and Machine Theory*, vol. 62, pp. 1–12, 2013. 6

[32] B. Han, "Variable impedance actuation using biphasic media," Ph.D. dissertation, University of Genova, 2013. 6, 12, 24, 25, 51

[33] X. Shen and M. Goldfarb, "Simultaneous force and stiffness control of a pneumatic actuator," *Journal of Dynamic Systems, Measurement, and Control*, vol. 129, no. 4, pp. 425–434, 2007. 6

[34] K. Bharadwaj, T. G. Sugar, J. B. Koeneman, and E. J. Koeneman, "Design of a robotic gait trainer using spring over muscle actuators for ankle stroke rehabilitation," *Journal of biomechanical engineering*, vol. 127, no. 6, pp. 1009–1013, 2005. 6

[35] W. Lim, S. H. Yeo, G. Yang, and I.-M. Chen, "Design and analysis of a cable-driven manipulator with variable stiffness," in *Robotics and Automation*

(ICRA), 2013 IEEE International Conference on. IEEE, 2013, pp. 4519–4524. 6, 59

[36] K. Yang, G. Yang, J. Wang, T. Zheng, and W. Yang, "Design analysis of a 3-dof cable-driven variable-stiffness joint module," in *Robotics and Biomimetics (ROBIO), 2015 IEEE International Conference on*. IEEE, 2015, pp. 529–534. 6

[37] G. A. Pratt and M. M. Williamson, "Series elastic actuators," in *Intelligent Robots and Systems 95.'Human Robot Interaction and Cooperative Robots', Proceedings. 1995 IEEE/RSJ International Conference on*, vol. 1. IEEE, 1995, pp. 399–406. 7

[38] G. A. Pratt, M. M. Williamson, P. Dillworth, J. Pratt, and A. Wright, "Stiffness isn't everything," in *experimental robotics IV*. Springer, 1997, pp. 253–262. 7

[39] "Mit's m2," http://www.ai.mit.edu/projects/leglab/robots/m2/m2.html, accessed: 2019-01-24. 7

[40] S. A. Migliore, E. A. Brown, and S. P. DeWeerth, "Biologically inspired joint stiffness control," in *Robotics and Automation, 2005. ICRA 2005. Proceedings of the 2005 IEEE International Conference on*. IEEE, 2005, pp. 4508–4513. 8

[41] "The amasc," http://www.msl.ri.cmu.edu/projects/actuator/, accessed: 2019-01-24. 8

[42] B. Verrelst, R. Van Ham, B. Vanderborght, F. Daerden, D. Lefeber, and J. Vermeulen, "The pneumatic biped "lucy" actuated with pleated pneumatic artificial muscles," *Autonomous Robots*, vol. 18, no. 2, pp. 201–213, 2005. 8

[43] B. Vanderborght, B. Verrelst, R. Van Ham, and D. Lefeber, "Controlling a bipedal walking robot actuated by pleated pneumatic artificial muscles," *Robotica*, vol. 24, no. 4, pp. 401–410, 2006. 8

[44] K. W. Hollander, T. G. Sugar, and D. E. Herring, "Adjustable robotic tendon using a'jack spring'/spl trade," in *Rehabilitation robotics, 2005. icorr 2005. 9th international conference on.* IEEE, 2005, pp. 113–118. 8

[45] R. Van Ham, M. Van Damme, B. Verrelst, B. Vanderborght, and D. Lefeber, "Maccepa, the mechanically adjustable compliance and controllable equilibrium position actuator: A 3dof joint with two independent compliances," *International Applied Mechanics*, vol. 43, no. 4, pp. 467–474, 2007. 8

[46] "Air springs information," https://www.globalspec.com/learnmore/mechanical˙components/springs/air˙springs, accessed: 2019-01-24. 14

[47] W. Bauer and H. Schwegler, "Hydro-pneumatic suspension system," May 22 2007, uS Patent 7,219,779. 14

[48] W. Bauer, *Hydropneumatic suspension systems.* Springer Science & Business Media, 2010. 14, 18, 21, 71, 72

[49] "Accumulators," https://www.hydraulicspneumatics.com/200/TechZone/Accumulators/Article/False/6446/TechZone-Accumulators, accessed: 2019-01-24. 17, 18

[50] "Accumulator types advantages," https://www.qualityhydraulics.com/blog/accumulator-types, accessed: 2019-01-24. 17

[51] "Hydraulic accumulators," https://www.hydac.com/de-en/products/hydraulic-accumulators.html, accessed: 2019-01-24. 17

[52] M. Ottestad, N. Nilsen, and M. R. Hansen, "Reducing the static friction in hydraulic cylinders by maintaining relative velocity between piston and cylinder," in *2012 12th International Conference on Control, Automation and Systems*, Oct 2012, pp. 764–769. 18, 72

[53] L. Le Tien, A. Albu-Schaffer, A. De Luca, and G. Hirzinger, "Friction observer and compensation for control of robots with joint torque measurement," in *Intelligent Robots and Systems, 2008. IROS 2008. IEEE/RSJ International Conference on.* IEEE, 2008, pp. 3789–3795. 18

[54] "Under, over and critical damping," https://ocw.mit.edu/courses/mathematics/18-03sc-differential-equations-fall-2011/unit-ii-second-order-constant-coefficient-linear-equations/damped-harmonic-oscillators/MIT18˙03SCF11˙s13˙2text.pdf, accessed: 2019-01-24. 20

[55] "Harmonic oscillator," https://en.wikipedia.org/wiki/Harmonic˙oscillator, accessed: 2019-01-24. 20

[56] "Simple harmonic motion, chapter 23," http://web.mit.edu/8.01t/www/materials/modules/chapter23.pdf, accessed: 2019-01-24. 20

[57] E. Jarzebowska, *Model-based tracking control of nonlinear systems*. Chapman and Hall/CRC, 2016. 25

[58] A. Umemura, Y. Saito, and K. Fujisaki, "A study on power-assisted rehabilitation robot arms operated by patient with upper limb disabilities," in *Rehabilitation Robotics, 2009. ICORR 2009. IEEE International Conference on*. IEEE, 2009, pp. 451–456. 32

[59] P. Maciejasz, J. Eschweiler, K. Gerlach-Hahn, A. Jansen-Troy, and S. Leonhardt, "A survey on robotic devices for upper limb rehabilitation," *Journal of neuroengineering and rehabilitation*, vol. 11, no. 1, p. 3, 2014. 32

[60] "Electro proportional valves," https://nem-hydraulics.com/products/directional-control-valves/, accessed: 2018-05-20. 41

[61] "Coils and connectors," https://nem-hydraulics.com/products/, accessed: 2018-05-20. 41

[62] "Standard bodies," https://nem-hydraulics.com/products/, accessed: 2018-05-20. 41

[63] "Digital electronic drivers e-ri-tes," https://www.automahydraulics.com.br/pdf/g210.pdf, accessed: 2018-05-20. 41

[64] "Pu5401 pressure sensor," https://www.ifm.com/it/en/product/PU5401, accessed: 2018-05-20. 41

[65] A. Caligiuri, "Design, implementation and experimental evaluation of a control system for a variable stiffness hydraulic actuator," Master's thesis, University of Genova, 2018. 42, 73

[66] X. DAUPTAIN, "Combination of force and speed/position control on different robotics axes," Master's thesis, University of Genova, 2016. 42, 73

[67] A. De Luca, F. Flacco, A. Bicchi, and R. Schiavi, "Nonlinear decoupled motion-stiffness control and collision detection/reaction for the vsa-ii variable stiffness device," in *Intelligent Robots and Systems, 2009. IROS 2009. IEEE/RSJ International Conference on.* IEEE, 2009, pp. 5487–5494. 49, 50

[68] B. Dániel, P. Korondi, and T. Thomessen, "Joint level collision avoidance for industrial robots," *IFAC Proceedings Volumes*, vol. 45, no. 22, pp. 655–658, 2012. 49

[69] S. Haddadin, A. De Luca, and A. Albu-Schäffer, "Robot collisions: A survey on detection, isolation, and identification," *IEEE Transactions on Robotics*, vol. 33, no. 6, pp. 1292–1312, 2017. 49, 50

[70] A. De Luca and R. Mattone, "Sensorless robot collision detection and hybrid force/motion control," in *Robotics and Automation, 2005. ICRA 2005. Proceedings of the 2005 IEEE International Conference on.* IEEE, 2005, pp. 999–1004. 50

[71] F. Flacco and A. De Luca, "Residual-based stiffness estimation in robots with flexible transmissions," in *Robotics and Automation (ICRA), 2011 IEEE International Conference on.* IEEE, 2011, pp. 5541–5547. 50

[72] S. Chen, M. Luo, and F. He, "A universal algorithm for sensorless collision detection of robot actuator faults," *Advances in Mechanical Engineering*, vol. 10, no. 1, p. 1687814017740710, 2018. 50

[73] A. De Luca and F. Flacco, "A pd-type regulator with exact gravity cancellation for robots with flexible joints," in *Robotics and Automation (ICRA), 2011 IEEE International Conference on.* IEEE, 2011, pp. 317–323. 52

[74] Y. Wang, G. Yang, K. Yang, C. Zhang, and T. Zheng, "Design optimization for a 2-dof cable-driven joint with large stiffness range," in *Industrial Electronics and Applications (ICIEA), 2017 12th IEEE Conference on.* IEEE, 2017, pp. 264–269. 58, 60

[75] E. A. Brackbill, Y. Mao, S. K. Agrawal, M. Annapragada, and V. N. Dubey, "Dynamics and control of a 4-dof wearable cable-driven upper arm exoskeleton," in *2009 IEEE International Conference on Robotics and Automation*, May 2009, pp. 2300–2305. 59

[76] X. Zhou, S.-k. Jun, and V. Krovi, "A cable based active variable stiffness module with decoupled tension," *Journal of Mechanisms and Robotics*, vol. 7, no. 1, p. 011005, 2015. 59, 60

[77] H. Jeong, B. Kang, and J. Cheong, "Stiffness analysis and experimental validation of modular-type hybrid antagonistic tendon-driven joint systems," *Robotica*, vol. 36, no. 11, pp. 1680–1700, 2018. 59, 60

[78] "Cylinder friction," https://it.mathworks.com/help/physmod/hydro/ref/cylinderfriction.html, accessed: 2019-01-24. 70

[79] S. Haddadin, A. Albu-Schaffer, A. De Luca, and G. Hirzinger, "Collision detection and reaction: A contribution to safe physical human-robot interaction," in *Intelligent Robots and Systems, 2008. IROS 2008. IEEE/RSJ International Conference on.* IEEE, 2008, pp. 3356–3363.